Collider phenomenology of Gauge-Higgs unification scenarios in warped extra dimensions

Marcela Carena,[1] Anibal D. Medina,[2,5] Boris Panes,[1,6] Nausheen R. Shah,[3,5] and Carlos E. M. Wagner[3,4,5]

[1]*Theoretical Physics Department, Fermi National Laboratory, Batavia, Illinois 60510, USA*
[2]*Department of Astronomy and Astrophysics, University of Chicago, 5640 South Ellis Avenue, Chicago, Illinois 60637, USA*
[3]*Enrico Fermi Institute, University of Chicago, 5640 South Ellis Avenue, Chicago, Illinois 60637, USA*
[4]*Kavli Institute for Cosmological Physics, University of Chicago, 5640 South Ellis Avenue, Chicago, Illinois 60637, USA*
[5]*HEP Division, Argonne National Laboratory, 9700 Cass Avenue, Argonne, Illinois 60439, USA*
[6]*Departamento de Física, Universidad Católica de Chile, Avenida V. Mackenna 4860, Santiago, Chile*

(Received 27 December 2007; published 3 April 2008)

We compute the couplings of the zero modes and first excited states of gluons, W's, Z gauge bosons, as well as the Higgs, to the zero modes and first excited states of the third generation quarks, in a Randall-Sundrum Gauge-Higgs unification scenario based on a bulk $SO(5) \times U(1)_X$ gauge symmetry, with gauge and fermion fields propagating in the bulk. Using the parameter space consistent with electroweak precision tests and radiative electroweak symmetry breaking, we study numerically the dependence of these couplings on the parameters of our model. Furthermore, after emphasizing the presence of light excited states of the top quark, which couple strongly to the Kaluza-Klein gauge bosons, the associated collider phenomenology is analyzed. In particular, we concentrate on the possible detection of the first excited state of the top, t^1, which tends to have a higher mass than the ones accessible via regular QCD production processes. We stress that the detection of these particles is still possible due to an increase in the pair production of t^1 induced by the first excited state of the gluon, G^1.

DOI: 10.1103/PhysRevD.77.076003 PACS numbers: 11.10.Kk, 11.15.Ex, 12.60.−i, 12.60.Cn

I. INTRODUCTION

Five-dimensional (5D) warped extra dimensions provide a very attractive beyond the standard model physics scenario, since the standard model (SM) weak scale-Planck scale hierarchy may be explained in a natural way [1]. The observed light quark and lepton masses, as well as the suppression of flavor violating operators, is naturally satisfied provided the quark and gauge fields propagate in the bulk and the first and second generation quark wave functions are suppressed towards the so-called infrared brane (IR brane), where the Higgs is localized and where the natural scale of energies is of the order of the weak scale [2–4].

The propagation of gauge and fermion fields in the bulk leads to the mixing of zero modes with Kaluza-Klein (KK) modes, which induces important tree-level effects on precision electroweak observables [5–7]. This happens especially for gauge bosons and third generation quarks [8–12]. The latter tend to be localized close to the IR brane in order to generate the large top-quark mass. The introduction of a custodial $SU(2)_R$ symmetry together with a discrete left-right symmetry leads to reduced corrections to the T parameter [13,14] and helps protect the bottom-quark coupling to the Z-gauge boson against large tree-level corrections. The top-bottom doublet may then be embedded in a bidoublet of the $SU(2)_L \times SU(2)_R$ group. Still, important corrections to the precision electroweak observables subsist at the one loop level, and agreement with data for KK masses at the reach of the LHC may only be obtained in a certain region of fermion mass bulk parameters of the third generation quarks [15,16].

The above requirements may be satisfied in a natural way by embedding the standard model gauge $SU(2)_L \times U(1)_Y$ group and the global custodial $SU(2)_R$ group into an $SO(5) \times U(1)_X$ gauge symmetry group [14]. The $SO(5) \times U(1)_X$ symmetry is broken by boundary conditions at the IR brane down to $SU(2)_L \times SU(2)_R \times U(1)_X$ and to $SU(2)_L \times U(1)_Y$ at the ultraviolet brane (UV brane). The five-dimensional components of the gauge bosons associated with the broken gauge symmetries at the IR brane have the proper quantum numbers of the Higgs doublet, leading to a natural implementation of the Gauge-Higgs unification mechanism [14–20]. In Ref. [21], the Coleman-Weinberg potential for the Higgs field was studied and its dependence on the five-dimensional mass parameters was determined. It was shown that the region of parameters consistent with precision electroweak observables is in good agreement with that required to obtain the breakdown of the electroweak symmetry, with the proper values of the top quark, bottom quark, and weak gauge boson masses.

One of the most important properties of these types of models is the existence of light excited states of the top quark. These quarks are strongly coupled to the gauge bosons KK modes which are localized towards the IR brane and are light enough so that the first KK mode of the gluon, G^1, tends to decay into them. This, in turn, leads to a reduced decay branching ratio of G^1 into top quarks. These properties, together with an increase in the width of G^1, make the G^1 detection via decay into top quarks more challenging than in the models which have been previously analyzed in the literature [22–24]. Moreover, for positive values of the bulk mass parameter associated with the

multiplet of the left-handed top-bottom doublet which is preferred by flavor constraints [25], the couplings of the left- and right-handed top quarks to G^1 become close to each other, leading to a reduced left-right top-quark production asymmetry. A similar effect will be present in the LHC phenomenology of the weak gauge bosons KK modes [26].

In this work, we shall concentrate on the production of the first excited state of the top quark t^1, at the LHC. We shall first show how to consistently determine the couplings of the quarks to gauge bosons in a functional way. These couplings will then be used to compute the decay widths and production cross section of the first top quark and gluon KK modes. We shall show that the presence of G^1 leads to an important enhancement of the t^1 production cross section for masses beyond the ones that can be tested via direct QCD production [27–30]. This is very important, since agreement with precision electroweak observables tends to be obtained for t^1 masses larger than 1 TeV, for which detection of t^1 via QCD production becomes very difficult. We shall also show that for large t^1-masses the branching ratios for the decay of t^1 into a W^+ and a bottom quark, a Z and a top quark, and a top quark and Higgs boson, are in an approximate 2:1:1 relation, as required by the Goldstone equivalence theorem. Moreover, we will show that the technique of massive jets [28,30] becomes very important for the reconstruction of the t^1 modes.

This article is organized as follows. In Sec. II we describe our 5-dimensional model. The mass spectrum and other relevant parameters of our model consistent with low energy data were investigated in Ref. [21]. In Secs. III and IV we will analyze how to obtain the properly normalized wave functions for the gauge fields and the fermions, respectively. In Sec. V we derive the various couplings necessary to study the collider phenomenology for this model and we numerically study the dependence of the calculated couplings on the parameters of our model, as well as the decay branching ratios. In Sec. VI we discuss the collider phenomenology. We reserve Sec. VII for our conclusions.

II. 5-DIMENSIONAL MODEL

We are interested in a 5D gauge theory with gauge group $SO(5) \times U(1)_X$. The geometry of our space-time will be that of Randall-Sundrum type I [1], with an orbifolded extra spatial dimension in the interval $x_5 \in [0, L]$. The metric for such a geometry is given by

$$ds^2 = a^2(x_5)\eta_{\mu\nu}dx^\mu dx^\nu - dx_5^2, \tag{1}$$

where $a(x_5) = e^{-kx_5}$. The space spanning the fifth dimension corresponds to a slice of AdS_5, with branes attached at the two boundary points: $x_5 = 0$ (UV brane) and $x_5 = L$ (IR brane).

We place our gauge fields, $A_M = A_M^\alpha T^\alpha$ and B_M, in the bulk, where T^α are the Hermitian generators of the fundamental representation of $SO(5)$ and generically $\mathrm{Tr}[\mathrm{T}^\alpha \cdot \mathrm{T}^\beta] = \mathrm{C}(5)\delta^{\alpha,\beta}$. The explicit form of the generators [17] are given in Appendix A. Our fermions ψ also live in the bulk, and they transform under a representation t^α of $SO(5)$.

The 5D action is

$$S_{5D} = \int d^4x \int_0^L dx_5 \sqrt{g}\Big(-\frac{1}{4g_5^2}\,\mathrm{Tr}\{F_{MN}F^{MN}\} - \frac{1}{4g_X^2}G_{MN}G^{MN} + \bar{\psi}(i\Gamma^N D_N - M)\psi\Big), \tag{2}$$

where $D_N = \partial_N - iA_N^\alpha t^\alpha - iB_N$ and g_5 and g_X are the 5D dimensionful gauge couplings.

The choice $C(5) = 1$ is a convenient choice, since it allows us to identify the eigenvalues of our generators as the weak isospin, with the four-dimensional coupling given by $g^2 = g_5^2/L$. Any other choice for $C(5)$ may be absorbed into a redefinition of the gauge fields or the gauge coupling leaving the physics unchanged.

To construct a realistic 4D low energy theory, we will break the 5D $SO(5) \times U(1)_X$ gauge symmetry down to the subgroup $SO(4) \times U(1)_Y = SU(2)_L \times SU(2)_R \times U(1)_Y$ on the IR brane and to $SU(2)_L \times U(1)_Y$ on the UV brane, where $Y/2 = T^{3_R} + Q_X$ is the hypercharge and Q_X is the $U(1)_X$ associated charge which is accommodated to obtain the correct hypercharge. We divide the generators of $SO(5)$ as follows: the generators of $SU(2)_{L,R}$ are denoted by $T^{a_{L,R}}$ and $t^{a_{L,R}}$, while the generators from the coset $SO(5)/SO(4)$ are denoted by $T^{\hat{a}}$ and $t^{\hat{a}}$.

In order to obtain the correct hypercharge and therefore the right Weinberg angle θ_W, we need to rotate the fields $A_M^{3_R} \in SU(2)_R$ and $B_M \in U(1)_X$ [18],

$$\begin{pmatrix} A_M^{\prime 3_R} \\ A_M^Y \end{pmatrix} = \begin{pmatrix} c_\phi & -s_\phi \\ s_\phi & c_\phi \end{pmatrix} \cdot \begin{pmatrix} A_M^{3_R} \\ B_M \end{pmatrix} \tag{3}$$

$$c_\phi \equiv \frac{g_5}{\sqrt{g_5^2 + g_X^2}}, \qquad s_\phi \equiv \frac{g_X}{\sqrt{g_5^2 + g_X^2}}. \tag{4}$$

The correct Weinberg angle is then given by $s_\phi^2 \simeq \tan^2\theta_W \simeq (0.23/0.77) \simeq 0.2987$. We will enforce A_μ^Y to have even parity, corresponding to the hypercharge gauge boson in the 4D low energy limit. From now on, we will drop the prime on $A^{\prime 3_R}$, and it will be understood that a_R refers to 1_R, 2_R, and $\prime 3_R$.

To implement the breaking of $SO(5)$ on the two branes as stated above, we impose the following boundary conditions on the gauge fields:

$$\partial_5 A_\mu^{a_L, Y} = A_\mu^{a_R, \hat{a}} = A_5^{a_L, Y} = 0, \qquad x_5 = 0 \tag{5}$$

$$\partial_5 A_\mu^{a_L, a_R, Y} = A_\mu^{\hat{a}} = A_5^{a_L, a_R, Y} = 0, \qquad x_5 = L. \tag{6}$$

As discussed in Ref. [21], this set of boundary conditions on the gauge fields leads to the identification of $A_5^{\hat{4}}$ as the

Higgs field with a nonvanishing vacuum expectation value (vev).

We concentrate on the third generation fermions which are the most important for electroweak symmetry breaking (EWSB) and electroweak precision test (EWPT) considerations. The SM fermions are embedded in full representations of the bulk gauge group as discussed in [15,16,21]. We therefore introduce in the quark sector three $SO(5)$ multiplets per generation as follows:

$$\begin{aligned}
\xi_{1L} \sim Q_{1L} &= \begin{pmatrix} \chi^u_{1L}(-,+)_{5/3} & q^u_L(+,+)_{2/3} \\ \chi^d_{1L}(-,+)_{2/3} & q^d_L(+,+)_{-1/3} \end{pmatrix} \\
&\quad \oplus u'_L(-,+)_{2/3}, \\
\xi_{2R} \sim Q_{2R} &= \begin{pmatrix} \chi^u_{2R}(-,+)_{5/3} & q'^u_R(-,+)_{2/3} \\ \chi^d_{2R}(-,+)_{2/3} & q'^d_R(-,+)_{-1/3} \end{pmatrix} \\
&\quad \oplus u_R(+,+)_{2/3}, \\
\xi_{3R} \sim Q_{3R} &= \begin{pmatrix} \chi^u_{3R}(-,+)_{5/3} & q''^u_R(-,+)_{2/3} \\ \chi^d_{3R}(-,+)_{2/3} & q''^d_R(-,+)_{-1/3} \end{pmatrix} \oplus T_{1R} \\
&= \begin{pmatrix} \psi'_R(-,+)_{5/3} \\ U'_R(-,+)_{2/3} \\ D'_R(-,+)_{-1/3} \end{pmatrix} \oplus T_{2R} \\
&= \begin{pmatrix} \psi''_R(-,+)_{5/3} \\ U''_R(-,+)_{2/3} \\ D_R(+,+)_{-1/3} \end{pmatrix},
\end{aligned} \tag{7}$$

where we show the decomposition under $SU(2)_L \times SU(2)_R$, and explicitly write the $U(1)_{EM}$ charges. The Qs are bidoublets of $SU(2)_L \times SU(2)_R$, with $SU(2)_L$ acting vertically and $SU(2)_R$ acting horizontally. T_1 and T_2 transform as $(\mathbf{3},\mathbf{1})$ and $(\mathbf{1},\mathbf{3})$ under $SU(2)_L \times SU(2)_R$, respectively, while u and u' are $SU(2)_L \times SU(2)_R$ singlets.

As was done in [21] we introduce mass mixing boundary terms,

$$\mathcal{L}_m = 2\delta(x_5 - L)[\bar{u}'_L M_{B_1} u_R + \bar{Q}_{1L} M_{B_2} Q_{3R} + \text{H.c.}], \tag{8}$$

where M_{B_1} and M_{B_2} are dimensionless masses. Since the Higgs mixes, amongst other terms, doublets with singlets, we see that with the current parity assignments for the singlet component of the first multiplet, we would in principle not have positive parity for this coupling at the IR brane. However, as discussed in [21], the switch in the singlet parity to $(+,+)$ is completely equivalent to taking $M^2_{B_1} \to 1/M^2_{B_1}$.

We also show the parities on the indicated 4D chirality, where $-$ and $+$ stands for odd and even parity conditions and the first and second entries in the bracket correspond to the parities in the UV and IR branes, respectively. Let us stress that, while odd parity is equivalent to a Dirichlet boundary condition, the even parity is a linear combination of Neumann and Dirichlet boundary conditions, that is determined via the fermion bulk equations of motion.

The boundary conditions for the opposite chirality fermion multiplet can be read off the ones above by a flip in both chirality and boundary condition, $(-,+)_L \to (+,-)_R$, for example. In the absence of mixing among multiplets satisfying different boundary conditions, the SM fermions arise as the zero modes of the fields obeying $(+,+)$ boundary conditions. The remaining boundary conditions are chosen so that $SU(2)_L \times SU(2)_R$ is preserved on the IR brane and so that mass mixing terms, necessary to obtain the SM fermion masses after electroweak symmetry breaking, can be written on the IR brane. Consistency of the above parity assignments with the original orbifold Z_2 symmetry at the IR brane was discussed in Ref. [21].

III. GAUGE FIELDS

Solving the equations of motion in the presence of the Higgs vev h is complicated, as these mix the Neumann and Dirichlet modes. However, 5D gauge symmetry relates these solutions to solutions with $h = 0$ [31]. These solutions, which we generally call $f^\alpha_G(x_5, 0)$, are related to the solutions in the presence of a Higgs vev, $f^\alpha_G(x_5, h)$, via simple gauge transformations:

$$f^\alpha_G(x_5, h) T^\alpha = \Omega^{-1}(x_5, h) f^\alpha_G(x_5, 0) T^\alpha \Omega(x_5, h), \tag{9}$$

where $\Omega(x_5, h)$ removes the vev h:

$$\Omega(x_5, h) = \exp\left[-iC_h h T^4 \int_0^{x_5} dy a^{-2}(y) \right], \tag{10}$$

and C_h is the Higgs normalization constant chosen such that the Higgs kinetic term is properly normalized, $C_h = g_5 (\int_0^L a^{-2})^{-1/2}$. Following the procedure outlined in [21] leads to the following wave functions for the gauge fields when $h = 0$, consistent with the UV boundary conditions:

$$\begin{aligned}
f^{a_L}_{G,n}(x_5, 0) &= C_{G,n,a_L} C(x_5, m_n), \\
f^{\hat{a}}_{G,n}(x_5, 0) &= C_{G,n,\hat{a}} S(x_5, m_n), \\
f^{Y}_{G,n}(x_5, 0) &= C_{G,n,Y} C(x_5, m_n), \\
f^{a_R}_{G,n}(x_5, 0) &= C_{G,n,a_R} S(x_5, m_n),
\end{aligned} \tag{11}$$

where the coefficients $C_{G,n,\alpha}$ are normalization constants and m_n is the particular KK mass under consideration. The functions $C[x_5, m_n]$ and $S[x_5, m_n]$ are the solutions to the equations of motion in the case of a vanishing Higgs vev, with the following initial conditions: $C(0, z) = 1$, $C'(0, z) = 0$, $S(0, z) = 0$, $S'(0, z) = z$. They are given by [32,33],

$$\begin{aligned}
C(x_5, z) = \frac{\pi z}{2k} a^{-1}(x_5) \Bigg[& Y_0\left(\frac{z}{k}\right) J_1\left(\frac{z}{k a(x_5)}\right) \\
& - J_0\left(\frac{z}{k}\right) Y_1\left(\frac{z}{k a(x_5)}\right) \Bigg]
\end{aligned} \tag{12}$$

$$S(x_5, z) = \frac{\pi z}{2k} a^{-1}(x_5)\left[J_1\left(\frac{z}{k}\right) Y_1\left(\frac{z}{ka(x_5)}\right) - Y_1\left(\frac{z}{k}\right) J_1\left(\frac{z}{ka(x_5)}\right)\right]. \quad (13)$$

We can now calculate $f^{\alpha}_{G,n}(x_5, h)$, the wave functions with $h \neq 0$, using Eq. (9). The explicit expressions for $f^{\alpha}_{G}(x_5, h)$ are given in Appendix B. The IR boundary conditions give us a system of algebraic equations for the coefficients $C_{G,n,\alpha}$. This system of equations can be broken into four subsets of dependent equations according to charge. The directions in internal space $\hat{1}$, 1_L, and 1_R and $\hat{2}$, 2_L, and 2_R mix and correspond to the components of $W^{+,-}$:

$$\sqrt{2}\cos\left[\frac{\lambda_G h}{f_h}\right] S[L] C_{G,\hat{i}} + \sin\left[\frac{\lambda_G h}{f_h}\right](S[L] C_{G,i_R} - C[L] C_{G,i_L}) = 0 \quad (14)$$

$$2(C_{G,i_L} C'[L] + C_{G,i_R} S'[L]) - \sqrt{2}\sin\left[\frac{\lambda_G h}{f_h}\right](e^{2kL} h C_h (C[L] C_{G,i_L} - S[L] C_{G,i_R}) - 2 C_{G,\hat{i}} S'[L]) + 2\cos\left[\frac{\lambda_G h}{f_h}\right](e^{2kL} h S[L] C_h C_{G,\hat{i}} + C_{G,i_L} C'[L] - C_{G,i_R} S'[L]) = 0 \quad (15)$$

$$2(C_{G,i_L} C'[L] + C_{G,i_R} S'[L]) + \sqrt{2}\sin\left[\frac{\lambda_G h}{f_h}\right](e^{2kL} h C_h (C[L] C_{G,i_L} - S[L] C_{G,i_R}) - 2 C_{G,\hat{i}} S'[L]) - 2\cos\left[\frac{\lambda_G h}{f_h}\right](e^{2kL} h S[L] C_h C_{G,\hat{i}} + C_{G,i_L} C'[L] - C_{G,i_R} S'[L]) = 0, \quad (16)$$

with $i = 1, 2$.

The neutral gauge bosons, Z and γ, are given by a mixture of $\hat{3}$, 3_L, $3_{R'}$, and Y:

$$\sqrt{2}\cos\left[\frac{\lambda_G h}{f_h}\right] S[L] C_{G,\hat{3}} + \sin\left[\frac{\lambda_G h}{f_h}\right](S[L] c_\phi C_{G,3_R} + C[L](s_\phi C_{G,Y} - C_{G,3_L})) = 0 \quad (17)$$

$$2(C_{G,3_L} + s_\phi C_{G,Y}) C'[L] + 2 c_\phi C_{G,3_R} S'[L] - \sqrt{2}\sin\left[\frac{\lambda_G h}{f_h}\right](e^{2kL} h C_h (-S[L] c_\phi C_{G,3_R} + C[L](C_{G,3_L} - s_\phi C_{G,Y})) - 2 C_{G,\hat{3}} S'[L]) + 2\cos\left[\frac{\lambda_G h}{f_h}\right](e^{2kL} h S[L] C_h C_{G,\hat{3}} + (C_{G,3_L} - s_\phi C_{G,Y}) C'[L] - c_\phi C_{G,3_R} S'[L]) = 0 \quad (18)$$

$$2 c_\phi (C_{G,3_L} - s_\phi C_{G,Y}) C'[L] + 2(1 + s_\phi^2) C_{G,3_R} S'[L] - \sqrt{2} c_\phi \sin\left[\frac{\lambda_G h}{f_h}\right](e^{2kL} h C_h (S[L] c_\phi C_{G,3_R} + C[L](-C_{G,3_L} + s_\phi C_{G,Y})) + 2 C_{G,\hat{3}} S'[L]) + 2 c_\phi \cos\left[\frac{\lambda_G h}{f_h}\right](-e^{2kL} h S[L] C_h C_{G,\hat{3}} + (-C_{G,3_L} + s_\phi C_{G,Y}) C'[L] + c_\phi C_{G,3_R} S'[L]) = 0 \quad (19)$$

$$2(s_\phi C_{G,3_L} + (1 + c_\phi^2) C_{G,Y}) C'[L] - 2 c_\phi s_\phi C_{G,3_R} S'[L] - \sqrt{2} s_\phi \sin\left[\frac{\lambda_G h}{f_h}\right](e^{2kL} h C_h (S[L] c_\phi C_{G,3_R} + C[L](-C_{G,3_L} + s_\phi C_{G,Y})) + 2 C_{G,\hat{3}} S'[L]) + 2 s_\phi \cos\left[\frac{\lambda_G h}{f_h}\right](-e^{2kL} h S[L] C_h C_{G,\hat{3}} + (-C_{G,3_L} + s_\phi C_{G,Y}) C'[L] + c_\phi C_{G,3_R} S'[L]) = 0. \quad (20)$$

Note that, in the above, we have dropped the mass dependence of the gauge boson wave functions, but it should be understood that m_n is taken to be the appropriate mass for the respective modes.

The procedure to obtain the normalization coefficients will be to drop one of the equations in the above subsets and solve for the normalization coefficients in terms of one of them, which can then be found by normalizing the related gauge field wave functions to unity. It is a combination of these wave functions which share the same charge that turns out to be the

true wave function for the particular gauge field under study. For example, explicitly for the W^+, dropping the first equation, we can solve for $C_{G,\hat{1}}$ and $C_{G,1_R}$ in terms of $C_{G,1_L}$:

$$C_{G,\hat{1}} = C_{G,1_L}\frac{-4\cos[\frac{\lambda_G h}{f_h}]C'[L]S'[L] + \sqrt{2}C_h a_L^{-2} h \sin[\frac{\lambda_G h}{f_h}](S[L]C'[L] + C[L]S'[L])}{2S'[L](C_h a_L^{-2} h\cos[\frac{\lambda_G h}{f_h}]S[L] + \sqrt{2}\sin[\frac{\lambda_G h}{f_h}]S'[L])}, \tag{21}$$

$$C_{G,1_R} = -C_{G,1_L}\frac{C'[L]}{S'[L]}, \tag{22}$$

where the ''Higgs decay constant'' is defined as

$$f_h^2 = \frac{1}{g_5^2\int_0^L dy a^{-2}(y)} \tag{23}$$

and $\lambda_G^2 = 1/2$.

By normalizing the wave functions which contribute to W^+, we find $C_{G,1_L}$ through

$$\int_0^L (|f_G^{\hat{1}}(x_5, h)|^2 + |f_G^{1_L}(x_5, h)|^2 + |f_G^{1_R}(x_5, h)|^2)dx_5 = 1 \tag{24}$$

or equivalently,

$$\int_0^L (|C_{G,\hat{1}} f_G^{\hat{1}}(x_5, 0)|^2 + |C_{G,1_L} f_G^{1_L}(x_5, 0)|^2 + |C_{G,1_R} f_G^{1_R}(x_5, 0)|^2)dx_5 = 1. \tag{25}$$

It is interesting to note that the explicit Higgs dependence in the normalization equations is always canceled. This is true for the gauge bosons as well as the fermions. Therefore the only dependence of these on the Higgs vev is through the normalization coefficients.

The condition that the entire system of equations, Eqs. (14)–(20), has a solution is only nontrivially realized if the determinant is zero. This gives us the spectrum of KK masses and was the main focus of Ref. [21]. The normalization coefficients must then be calculated using the procedure defined above. Once all the normalization constants have been computed, we have all the information necessary to calculate the wave functions for the gauge bosons with the appropriate masses. However, we would like to point out a subtlety in the neutral sector where after electroweak symmetry breaking we obtain the Z gauge boson and the photon. In principle, dropping any of the four equations and solving the other three should give us the same result. However, since the Higgs does not couple to the photon, the photon does not have any component in the $\hat{3}$ and 3_R directions. Therefore, dropping either $f_G^{\hat{3}}(L, h) = 0$ or $f_G^{3_R}(L, h) = 0$ does not lead to the photon solution in the massless limit. To compute the coefficients associated with the photon, we need to drop the boundary condition for either $f_G^{3_L}(L, h)$ or $f_G^{Y}(L, h)$. In this case the $C_{G,\alpha}$ are given by

$$C_{G,\hat{3}} = C_{G,3_L}\frac{C'[L](c_\phi^2 a_L^{-2} z\sin[\frac{\lambda h}{f_h}] - 2C[L]S'[L]\cot[\frac{\lambda h}{2f_h}])}{\sqrt{2}S'[L](a_L^{-2} z\cos[\frac{\lambda h}{f_h}] + C[L]S'[L])} \tag{26}$$

$$C_{G,3_R} = -C_{G,3_L}\frac{c_\phi C'[L]}{S'[L]}, \tag{27}$$

$$C_{G,Y} = C_{G,3_L}\frac{(a_L^{-2} z\cos[\frac{\lambda h}{f_h}] - (1 + s_\phi^2 - \csc^2[\frac{\lambda h}{2f_h}])S[L]C'[L] + C[L]S'[L])}{s_\phi(a_L^{-2} z\cos[\frac{\lambda h}{f_h}] + C[L]S'[L])}, \tag{28}$$

where we have used the Wronskian relation,

$$S'(x_5, z)C(x_5, z) - S(x_5, z)C'(x_5, z) = z a(x_5)^{-2}. \tag{29}$$

The consistency of this procedure can be seen by the fact that in this case in the massless limit $f_G^{\hat{3}}(x_5, h)$, Eq. (B4), and $f_G^{3'_R}(x_5, h)$, a combination of Eqs. (B6) and (B7), are identically zero as we expect for the photon field.

IV. FERMIONIC KK PROFILES

With the introduction of mass mixing boundary terms, Eq. (8), and through the Higgs vev, the different multiplets are now related via the equations of motion. The details of the calculations for the fermion wave functions and their boundary conditions were discussed thoroughly in Ref. [21]. The fermion vector functions in the $h = 0$ gauge and the IR boundary conditions used to calculate the co-

efficients $C_{F,i}$ may be determined in a similar way as for the gauge bosons.

Our three fermion multiplets in the $h = 0$ gauge can be arranged in vector functions in the following way:

$$f_{F,1,L}(x_5,0) = \begin{bmatrix} C_{F,1}S_{M_1} \\ C_{F,2}S_{M_1} \\ C_{F,3}\dot{S}_{-M_1} \\ C_{F,4}\dot{S}_{-M_1} \\ C_{F,5}S_{M_1} \end{bmatrix}$$

$$f_{F,2,R}(x_5,0) = \begin{bmatrix} C_{F,6}S_{-M_2} \\ C_{F,7}S_{-M_2} \\ C_{F,8}S_{-M_2} \\ C_{F,9}S_{-M_2} \\ C_{F,10}\dot{S}_{M_2} \end{bmatrix} \tag{30}$$

$$f_{F,3,R}(x_5,0) = \begin{bmatrix} C_{F,11}S_{-M_3} \\ C_{F,12}S_{-M_3} \\ C_{F,13}S_{-M_3} \\ C_{F,14}S_{-M_3} \\ C_{F,15}S_{-M_3} \\ C_{F,16}S_{-M_3} \\ C_{F,17}S_{-M_3} \\ C_{F,18}S_{-M_3} \\ C_{F,19}S_{-M_3} \\ C_{F,20}\dot{S}_{M_3} \end{bmatrix},$$

where, as for the gauge bosons, the $C_{F,i}$ are normalization constants. The opposite chiralities have opposite boundary conditions and can be read from these ones. The solutions to the fermion equations of motion in the h = 0 gauge are written in terms of [32]:

$$\tilde{S}_M(x_5,z) = \frac{\pi z}{2k} a^{-c-(1/2)}(x_5) \times \left[J_{(1/2)+c}\left(\frac{z}{k}\right) Y_{(1/2)+c}\left(\frac{z}{ka(x_5)}\right) - Y_{(1/2)+c}\left(\frac{z}{k}\right) J_{(1/2)+c}\left(\frac{z}{ka(x_5)}\right)\right], \tag{31}$$

which has initial conditions $\tilde{S}_M(0,z) = 0$, $\partial_5 \tilde{S}_{\pm M}(0,z) = z$. The fermion wave function solutions with $h = 0$, Eq. (30), are related to the functions in Eq. (31) via

$$S_{\pm M}(x_5,z) = \frac{e^{\pm M x_5}}{a^2(x_5)} \tilde{S}_{\pm M}(x_5,z), \tag{32}$$

$$\dot{S}_{\pm M}(x_5,z) = \mp \frac{e^{\pm M x_5}}{z a(x_5)} \partial_5 \tilde{S}_{\pm M}(x_5,z). \tag{33}$$

The normalization of the fermion wave functions for the free fermion case contains a nontrivial dependence on the warp factor,

$$\int_0^L dx_5 a(x_5)^3 f^i_{F,m_n,(L,R)}(x_5,0) f^i_{F,m_m,(L,R)}(x_5,0) = \delta_{m,n}, \tag{34}$$

where here $f^i_{F,m_n,(L,R)}(x_5,0)$ is proportional to either $S_M(x_5,m_n)$ or $\dot{S}_M(x_5,m_n)$ and in this case, m_n is the mass spectrum in the free fermion case. The superscript i, which denotes the vector component, is not being summed over and we denote the chiral indices as L, R for left-handed and right-handed fields. It is therefore convenient to eliminate the dependence on $a(x_5)$ of the normalization condition by redefining the functions

$$S_{\pm M} \to a(x_5)^{-3/2} S_{\pm M}, \qquad \dot{S}_{\pm M} \to a(x_5)^{-3/2} \dot{S}_{\pm M}, \quad \text{or}$$
$$f^i_{F,m_n,(L,R)} \to a(x_5)^{-3/2} f^i_{F,m_n,(L,R)}. \tag{35}$$

In the following, we shall apply this redefinition, which allows for a clearer interpretation of the localization of the fermion wave functions in the fifth dimension and maintains the validity of the functional relations given in Eq. (30).

We can write the final fermion vector functions in the presence of the vev h using the same gauge transformation as for the gauge bosons:

$$f_{F,1,L}(x_5,h) = \Omega f_{F,1,L}(x_5,0) \tag{36}$$

$$f_{F,2,R}(x_5,h) = \Omega f_{F,2,R}(x_5,0) \tag{37}$$

$$f_{F,3,R}(x_5,h) = \Omega f_{F,3,R}(x_5,0). \tag{38}$$

Applying the boundary conditions at $x_5 = L$, taking into account the mass mixing terms from Eq. (8) we derive the conditions on $f_F(L,h)$:

$$f^{1,\ldots,4}_{F,1,R} + M_{B_2} f^{1,\ldots,4}_{F,3,R} = 0 \qquad f^5_{F,1,R} + M_{B1} f^5_{F,2,R} = 0$$
$$f^{1,\ldots,4}_{F,2,L} = 0 \qquad f^{1,\ldots,4}_{F,3,L} - M_{B_2} f^{1,\ldots,4}_{F,1,L} = 0 \tag{39}$$
$$f^5_{F,2,L} - M_{B_1} f^5_{F,1,L} = 0 \qquad f^{5,\ldots,10}_{F,3,L} = 0,$$

where the superscripts denote the vector components.

Asking that the determinant of this system of equations vanishes so that we get a nontrivial solution, we obtain the spectrum of the fermion modes [21]. We note here that the same value $\lambda_F = 1/\sqrt{2}$ is found in the fermionic case as for gauge bosons.

To find the normalization coefficients for the fermion wave functions, we use the same procedure as for the gauge bosons: solving the equations for the boundary conditions at $x_5 = L$ and then normalizing the fermions coupled via the Higgs and boundary mass mixing terms. The equations are presented in Appendix B. In the equations as well as in the solutions, the functions are evaluated at the IR boundary, $x_5 = L$. For the charge 5/3 fermions, the coefficients are

$$C_{F,11} = C_{F,1} \frac{M_{B_2} S_{M_1}}{\dot{S}_{-M_3}} \cos\left[\frac{\lambda_F h}{f_h}\right] \tag{40}$$

$$C_{F,15} = C^*_{F,18} = \frac{i}{\sqrt{2}} C_{F,1} \frac{M_{B_2} S_{M_1}}{\dot{S}_{-M_3}} \sin\left[\frac{\lambda_F h}{f_h}\right]. \quad (41)$$

Charge $-1/3$ fermions:

$$C_{F,14} = C_{F,4} \cos\left[\frac{\lambda_F h}{f_h}\right] \frac{M_{B_2} \dot{S}_{-M_1}}{\dot{S}_{-M_3}} \quad (42)$$

$$C_{F,17} = -\frac{S_{M_3}}{\dot{S}_{-M_3}} C_{F,20} = \frac{i}{\sqrt{2}} C_{F,4} \sin\left[\frac{\lambda_F h}{f_h}\right] \frac{M_{B_2} \dot{S}_{-M_1}}{\dot{S}_{-M_3}}. \quad (43)$$

Charge $2/3$ fermions:

$$C_{F,3} = C_{F,2} \frac{M^2_{B_2} S_{M_1} S_{-M_3} + \dot{S}_{M_1} \dot{S}_{-M_3}}{M^2_{B_2} S_{-M_3} \dot{S}_{-M_1} + S_{-M_1} \dot{S}_{-M_3}} \quad (44)$$

$$C_{F,5} = \sqrt{2} C_{F,2} \cot\left[\frac{\lambda_F h}{f_h}\right] \quad (45)$$

$$\begin{aligned} C_{F,7} = C_{F,8} &= \frac{S_{M_2}}{\sqrt{2}\dot{S}_{-M_2}} \tan\left[\frac{\lambda_F h}{f_h}\right] C_{F,10} \\ &= -\frac{1}{2} C_{F,2} S_{M_2} \frac{M^2_{B_2} S_{-M_3} (2\dot{S}_{-M_1}\dot{S}_{M_1} - \sin[\frac{\lambda_F h}{f_h}]^2 (\dot{S}_{-M_1}\dot{S}_{M_1} - S_{-M_1} S_{M_1})) + 2 S_{-M_1}\dot{S}_{M_1}\dot{S}_{-M_3}}{M_{B_1} (\sin[\frac{\lambda_F h}{f_h}]^2 S_{-M_2} S_{M_2} + \cos[\frac{\lambda_F h}{f_h}]^2 \dot{S}_{-M_2}\dot{S}_{M_2})(M^2_{B_2} S_{-M_3}\dot{S}_{-M_1} + S_{-M_1}\dot{S}_{-M_3})} \end{aligned} \quad (46)$$

$$C_{F,12} = -\frac{\sin[\frac{\lambda_F h}{f_h}]^2}{1 + \cos[\frac{\lambda_F h}{f_h}]^2} C_{F,13} = -\frac{1}{2} C_{F,2} M_{B_2} \sin\left[\frac{\lambda_F h}{f_h}\right]^2 \frac{\dot{S}_{-M_1}\dot{S}_{M_1} - S_{-M_1} S_{M_1}}{M^2_{B_2} S_{-M_3}\dot{S}_{-M_1} + S_{-M_1}\dot{S}_{-M_3}} \quad (47)$$

$$C_{F,16} = C^*_{F,19} = \frac{i}{2} C_{F,2} M_{B_2} \sin\left[\frac{\lambda_F h}{f_h}\right] \cos\left[\frac{\lambda_F h}{f_h}\right] \frac{\dot{S}_{-M_1}\dot{S}_{M_1} - S_{-M_1} S_{M_1}}{M^2_{B_2} S_{-M_3}\dot{S}_{-M_1} + S_{-M_1}\dot{S}_{-M_3}}. \quad (48)$$

Again, as for the gauge bosons, we can use the normalization conditions to solve for the coefficients $C_{F,i}$,

$$\int_0^L \sum_i f^{Q*}_{F,i,m_n,(L,R)}(x_5, h) \cdot f^{Q}_{F,i,m_n,(L,R)}(x_5, h) dx_5 = 1, \quad (49)$$

where the index i takes into account the sum over the three different multiplets and the superscript Q denotes the charge of the fermion state. Here m_n denotes the masses of the zero and KK modes fermions of charge Q. We define the vector $f^Q_F(x_5, h)$ as the vector $f_F(x_5, h)$ with all components which do not participate in the state mixing set to zero. Using the equations of motion for the fermion fields and the boundary conditions associated with them, one can show that, once one imposes the normalization condition for one chirality, the other one is automatically satisfied. We checked the consistency of our analysis by numerically verifying the above statement.

V. COUPLINGS

Once we have the solutions for all the normalization coefficients, we have the necessary information to compute the various boson-fermion couplings. We will start with the coupling of the first excited state of the gluon field G^1 with the fermions. Since gluons do not interact with the Higgs field, their profile on the fifth dimension is given by $C[x_5, z]$, where in this case $z = m_{G^1}$ is the G^1-mass. For G^1-induced pair production of t^1's and for backgrounds to this production mechanism, we are interested in the $g_{G^1\bar{t}^1 t^1}$, $g_{G^1\bar{t}t}$, and $g_{G^1\bar{t}t^1}$ couplings. Since the profiles in the 5th dimension of left-handed and right-handed fields differ, this leads to left-handed and right-handed couplings which are different. Similar to the description given in Eq. (2) for the electroweak interactions, these couplings proceed from the covariant derivatives in the fermion kinetic terms,

$$\begin{aligned} g_{G^1\bar{t}t} = g_{5s} N_{G^1} \int_0^L \left(\sum_i f^{2/3*}_{F,i,m_t}(x_5, h) \cdot f^{2/3}_{F,i,m_t}(x_5, h) \right) \\ \times C[x_5, m_{G^1}] dx_5, \end{aligned} \quad (50)$$

where to simplify notation we omit the chiral subindices. Furthermore, in the above expression g_{5s} is the 5D strong coupling related to the 4D strong gauge coupling by $g_s = g_{5s}/\sqrt{L}$ and N_{G^1} is the normalization for G^1, which is given by

$$N_{G^1} = \left(\int_0^L C^2[x_5, m_{G^1}] dx_5 \right)^{-1/2}. \quad (51)$$

To obtain $g_{G^1\bar{t}^1 t^1}$ and $g_{G^1\bar{t}^1 t}$ we only need to replace m_t by the appropriate fermion mass in Eq. (50).

Likewise, we calculate the Higgs-fermion coupling $g_{H\bar{t}t^1}$, which will be important when studying the decay modes of t^1 to Higgs and tops. We look again at the kinetic term for the fermions. The Higgs originates from the zero mode of the $A^{\hat{4}}_5$ gauge field which enters in the fermion covariant derivative. Thus the coupling, which mixes left

and right-handed fields (left-right or right-left), takes the form

$$
\begin{aligned}
g_{H\bar{t}t^1} &= iC_h \int_0^L \left(\sum_i f^{*2/3}_{F,i,m_t}(x_5,h) f_H \cdot T^{\hat{4}} \cdot f^{2/3}_{F,i,m_{t^1}}(x_5,h) \right) e^{-kx_5} dx_5 \\
&= i\frac{C_h}{2} C_{F,2,1} C^*_{F,2,0} \int_0^L e^{-kx_5} \Big(if_H f^*_{F,5,0}(f_{F,2,1} + f_{F,3,1}) - i(f^*_{F,2,0} + f^*_{F,3,0}) f_H f_{F,5,1} + if_H f^*_{F,10,0}(f_{F,7,1} + f_{F,8,1}) \\
&\quad - i(f^*_{F,7,0} + f^*_{F,8,0}) f_H f_{F,10,1} + (f^*_{F,16,0} - f^*_{F,19,0}) \frac{f_H f_{F,12,1}}{\sqrt{2}} + (f^*_{F,16,0} - f^*_{F,19,0}) \frac{f_H f_{F,13,1}}{\sqrt{2}} \\
&\quad + (f^*_{F,12,0} + f^*_{F,13,0}) \frac{f_H f_{F,16,1}}{\sqrt{2}} - (f^*_{F,12,0} + f^*_{F,13,0}) \frac{f_H f_{F,19,1}}{\sqrt{2}} \Big),
\end{aligned} \tag{52}
$$

where $f_H = e^{2kx_5}$ is the Higgs profile and C_h is the Higgs field normalization. For simplicity we have written $f_{F,i,m_t} = f_{F,i,0}$, $f_{F,i,m_{t^1}} = f_{F,i,1}$ and we again omit the chiral indices. The subscripts 0 and 1 on the C's and the fermion functions denote the fermion mass that should be used, m_t or m_{t^1}, respectively. Using relationships between the fermion normalization coefficients given in Appendix B, this can be written as

$$
\begin{aligned}
g_{H\bar{t}t^1} &= \frac{C_h}{2} \int_0^L dx e^{kx_5} (C_{F,3,0} C_{F,5,1} S_{-M_1,0} S_{M_1,1} - (C_{F,5,0} C_{F,2,1} - C_{F,2,0} C_{F,5,1}) \dot{S}_{M_1,0} S_{M_1,1} \\
&\quad + 2(C_{F,7,0} C_{F,10,1} S_{-M_2,0} S_{M_2,1} - C_{F,10,0} C_{F,7,1} \dot{S}_{M_2,0} \dot{S}_{-M_2,1}) + i\sqrt{2}(C^*_{F,16,0}(C_{F,12,1} + C_{F,13,1}) \\
&\quad + C_{F,5,0} C_{F,3,1} \dot{S}_{M_1,0} \dot{S}_{-M_1,1} + (C_{F,12,0} + C_{F,13,0}) C_{F,16,1}) S_{-M_3,0} \dot{S}_{-M_3,1}).
\end{aligned} \tag{53}
$$

In the above, the only explicit dependence of the couplings on the Higgs vev comes through the fermion normalization coefficients.

For the case of $g_{H\bar{t}t}$ or $g_{H\bar{t}^1t^1}$, the Higgs couplings take a particularly simple form,

$$
\begin{aligned}
g_{H\bar{t}t} &= \frac{C_h}{2} \int_0^L e^{kx_5} (C_{F,3,0} C_{F,5,0} (\dot{S}_{M_1,0}[x_5] \dot{S}_{-M_1,0}[x_5] - S_{M_1,0}[x_5] S_{-M_1,0}[x_5]) + 2C_{F,7,0} C_{F,10,0} (\dot{S}_{M_2,0}[x_5] \dot{S}_{-M_2,0}[x_5] \\
&\quad - S_{M_2,0}[x_5] S_{-M_2,0}[x_5])) dx_5 \\
&= -\frac{C_h}{2} \int_0^L e^{2kx_5} (C_{F,3,0} C_{F,5,0} + 2C_{F,7,0} C_{F,10,0}) dx_5,
\end{aligned} \tag{54}
$$

where we have used the Crowian relation:

$$
-\dot{S}_M(x_5,z)\dot{S}_{-M}(x_5,z) + S_M(x_5,z) S_{-M}(x_5,z) = 1/a(x_5). \tag{55}
$$

In the case of $g_{H\bar{t}^1t^1}$, we obtain a similar result with the subindex 0 replaced by 1.

Another important coupling which will be of major interest for the reconstruction of the t^1 invariant mass, as will be seen in the collider section, is the $g_{W^+\bar{t}^1b}$ coupling which again comes from the covariant kinetic term of the fermion fields, and is given by

$$
\begin{aligned}
g_{W^+\bar{t}^1b} &= \sqrt{2} g_5 \int_0^L \left(\sum_{i,\alpha} f^{2/3*}_{F,i,m_{t^1}}(x_5,h) \cdot (f_{G\alpha}(x_5,h) T^\alpha) \cdot f^{1/3}_{F,i,m_b}(x_5,h) \right) dx_5 \\
&= g_5 C_{G,5} \int_0^L \Big[\frac{C^*_{F,2,1} C_{F,4,0}}{2} \Big(f_{G,8} f^*_{F,2,1} f_{F,4,0} - f_{G,5} f^*_{F,3,1} f_{F,4,0} - f_{G,1} f^*_{F,5,1} f_{F,4,0} + if_{G,5} f^*_{F,12,1} f_{F,17,0} \\
&\quad + f_{G,1} f^*_{F,13,1} f_{F,14,0} + \Big(-\frac{i}{\sqrt{2}} f_{G,5} f_{F,14,0} + \frac{1}{\sqrt{2}} f_{G,1} f_{F,17,0} \Big) f^*_{F,16,1} + if_{G,8} f^*_{F,12,1} f_{F,14,0} + f_{G,5} f^*_{F,13,1} f_{F,20,0} \\
&\quad + \Big(-\frac{i}{\sqrt{2}} f_{G,5} f_{F,14,0} + \frac{1}{\sqrt{2}} f_{G,8} f_{F,20,0} \Big) f^*_{F,19,1} \Big) \Big],
\end{aligned} \tag{56}
$$

where these couplings are left-left and right-right, g_5 is the 5D weak coupling, and for simplicity we have written $f_{G\alpha}(x_5,h) = f_{G,\alpha}$. Here α runs over the generators associated with the W boson: $\hat{1}$, 1_L, and 1_R. The subindex 0 refers to the bottom quark and the subindex 1 to t^1. Notice that in this case the second multiplet does not contribute to the coupling since it does not mix to form the bottom 5D profile. The first excited state of the bottom fermion has a mass that puts it out of reach for the LHC.

The $g_{Z\bar{t}^1 t}$ coupling, which is also important as a decay channel for t^1, is similarly given by

$$
\begin{aligned}
g_{Z\bar{t}^1 t} &= g_5 \int_0^L \left(\sum_{i,\alpha} f^{*2/3}_{F,i,m_{t^1}}(x_5,h) \cdot (f^{\alpha}_G(x_5,h) T^{\alpha}) \cdot f^{2/3}_{F,i,m_t}(x_5,h) + \text{H.c.} \right) dx_5 \\
&= g_5 C_{G,7} \int_0^L \Bigg[\frac{C_{F,2,0} C^*_{F,2,1}}{2} \Bigg(\left(\left(\frac{4g_X}{3g_5} \right) f_{G,11} - f_{G,7} + f_{G,10} \right) f_{F,2,0} f^*_{F,2,1} + f_{G,3} f_{F,2,0} f^*_{F,5,1} \\
&\quad + \left(\left(\frac{4g_X}{3g_5} \right) f_{G,11} + f_{G,7} - f_{G,10} \right) f_{F,3,0} f^*_{F,3,1} - f_{G,3} f_{F,7,0} f^*_{F,10,1} + f_{G,3} f_{F,8,0} f^*_{F,10,1} \\
&\quad + \left(-f_{G,3} f^*_{F,2,1} + f_{G,3} f^*_{F,3,1} + \left(\frac{4g_X}{3g_5} \right) f_{G,11} f^*_{F,5,1} \right) f_{F,5,0} + f_{G,3} f_{F,3,0} f^*_{F,5,1} \\
&\quad + \left(\left(\frac{4g_X}{3g_5} \right) f_{G,11} - f_{G,7} + f_{G,10} \right) f_{F,7,0} f^*_{F,7,1} + \left(\left(\frac{4g_X}{3g_5} \right) f_{G,11} + f_{G,7} - f_{G,10} \right) f_{F,8,0} f^*_{F,8,1} \\
&\quad + \left(-f_{G,3} f^*_{F,7,1} + f_{G,3} f^*_{F,8,1} + \left(\frac{4g_X}{3g_5} \right) f_{G,11} f^*_{F,10,1} \right) f_{F,10,0} + \left(\left(\left(\frac{4g_X}{3g_5} \right) f_{G,11} - f_{G,7} + f_{G,10} \right) f^*_{F,12,1} + \frac{i}{\sqrt{2}} f_{G,3} f^*_{F,16,1} \right. \\
&\quad \left. - \frac{i}{\sqrt{2}} f_{G,3} f^*_{F,19,1} \right) f_{F,12,0} + \left(\left(\left(\frac{4g_X}{3g_5} \right) f_{G,11} + f_{G,7} - f_{G,10} \right) f^*_{F,13,1} - \frac{i}{\sqrt{2}} f_{G,3} f^*_{F,16,1} + \frac{i}{\sqrt{2}} f_{G,3} f^*_{F,19,1} \right) f_{F,13,0} \\
&\quad + \left(\left(\frac{4g_X}{3g_5} \right) f_{G,11} f^*_{F,16,1} + \frac{i}{\sqrt{2}} f_{G,3} f^*_{F,13,1} - \frac{i}{\sqrt{2}} f_{G,3} f^*_{F,12,1} \right) f_{F,16,0} + \left(\left(\frac{4g_X}{3g_5} \right) f_{G,11} f^*_{F,19,1} + \frac{i}{\sqrt{2}} f_{G,3} f^*_{F,12,1} \right. \\
&\quad \left. - \frac{i}{\sqrt{2}} f_{G,3} f^*_{F,13,1} \right) f_{F,19,0} \Bigg) \Bigg],
\end{aligned}
\tag{57}
$$

where α runs over $\hat{3}$, 3_L, 3_R, Y, and we introduce $T^Y = Q_X I = \frac{2}{3}\frac{g_X}{g_5} \mathrm{I}$.

The functional dependence of the couplings does not change with KK states. The standard model couplings may be obtained from the above expressions by replacing the appropriate mass. We have evaluated numerically the couplings g_{Gtt}, g_{Htt}, g_{Wtb}, and g_{Ztt} for the would be zero mode masses of all the fields and recovered the standard model results, as expected, with slight modifications coming from the mixing with the KK states which become smaller as h becomes much smaller than $\tilde{k}$, where $\tilde{k} \equiv ke^{-kL}$ gives the characteristic scale of the KK masses.

A. Couplings in the linear regime

The linear regime is defined as the parameter space of our model where $\lambda h/f_h < 0.35$. As discussed in Ref. [21], all KK masses become larger than the SM particle masses in this regime. The fermion solution, Eq. (31), for $z \ll \tilde{k}$ takes the form

$$
\tilde{S}_M \approx z \int_0^{x_5} a^{-1}(x_5) e^{-2My} dy + \mathcal{O}(z^3). \tag{58}
$$

Keeping only up to linear order in h and z, we can use the last expression in Eq. (54) for $g_{H\bar{t}t}$ and see that in this limiting case this coupling reduces to

$$
g_{H\bar{t}t} \approx \frac{m_t}{h} = \frac{y_{\text{top}}}{\sqrt{2}} \tag{59}
$$

recovering the expression for the top Yukawa coupling, y_{top}. Similarly, we can obtain analytical expressions for the $g_{W^+\bar{t}^1_L b_L}$, $g_{Z\bar{t}^1_L t_L}$, and $g_{H\bar{t}^1_R t_L}$ couplings in the low energy limit which will be of importance when analyzing branching ratios for the decay of t^1. Since the mass of t^1 is smaller than $\tilde{k}$, one can use an expansion similar to Eq. (58) to obtain the previously mentioned couplings. We find the following approximate expressions:

$$
g_{W^+\bar{t}^1_L b_L} \approx \frac{g^2}{4} \left(\frac{h}{m_{t^1}} \right) M_{B_1} \left(\frac{\tilde{k}}{m_{t^1}} \right) \left(1 + \frac{1}{2(1+2c_1)} \left(\frac{m_{t^1}}{\tilde{k}} \right)^2 \right) \frac{(1+2c_1)(1+2c_2)\sqrt{kL}\sqrt{(1-2c_1)(3+2c_1)(3+2c_2)}}{\sqrt{((1+2c_1)^2(3+2c_1) + M^2_{B_1}(1+2c_2)^2(3+2c_2))}} \tag{60}
$$

$$
g_{Z\bar{t}^1_L t_L} \approx \frac{g_{W^+\bar{t}^1_L b_L}}{\sqrt{2}} \sqrt{1 + s^2_\phi} \tag{61}
$$

$$
g_{H\bar{t}^1_R t_L} \approx \frac{\sqrt{2} m_{t^1}}{gh} g_{W^+\bar{t}^1_L b_L}. \tag{62}
$$

Notice that the appearance in $g_{W^+\bar{t}^1_L b_L}$ and $g_{Z\bar{t}^1_L t_L}$ of an additional power of g, as well as the dependence on h/m_{t^1}, has to do with mixing of the charge 2/3 states through Yukawa coupling interactions proportional to h. These approximate expressions are in good agreement with numerical values obtained for the full couplings.

The decay widths of G^1 to fermions and the decay widths of t^1 to Wb, Zt, and Ht are given by

$$\Gamma_{G^1tt} = \frac{m_{G^1}}{48\pi}\sqrt{1-4\frac{m_t^2}{m_{G^1}^2}}\left(g^2_{G^1\bar{t}_L t_L} + g^2_{G^1\bar{t}_R t_R} - (g^2_{G^1\bar{t}_L t_L} + g^2_{G^1\bar{t}_R t_R} - 6g_{G^1\bar{t}_L t_L} g_{G^1\bar{t}_R t_R})\frac{m_t^2}{m_{G^1}^2}\right) \tag{63}$$

$$\Gamma_{Wt^1b} = \frac{g^2_{W^+\bar{t}^1_L b_L}}{32\pi}\frac{m^3_{t^1}}{m^2_W}\left(1-3\frac{m_W^4}{m_{t^1}^4}+2\frac{m_W^6}{m_{t^1}^6}\right) \tag{64}$$

$$\Gamma_{Zt^1t} = \frac{1}{8\pi}f(m_{t^1}, m_Z, m_t)\frac{m^2_{t^1}}{m_Z^2}\left(\frac{g^2_{Z\bar{t}^1_L t_L} + g^2_{Z\bar{t}^1_R t_R}}{2}\left(1+\frac{m_Z^2}{m^2_{t^1}}+\frac{m_Z^2 m_t^2}{m_{t^1}^4}+\frac{m_t^4}{m_{t^1}^4}-2\frac{m_t^2}{m^2_{t^1}}-2\frac{m_Z^4}{m_{t^1}^4}\right)-6g_{Z\bar{t}^1_L t_L}g_{Z\bar{t}^1_R t_R}m_Z^2\frac{m_t}{m^3_{t^1}}\right) \tag{65}$$

$$\Gamma_{Ht^1t} = \frac{1}{8\pi m^2_{t^1}}f(m_{t^1}, m_t, m_H)\left(\frac{(g^2_{Ht^1_L t_R} + g^2_{Ht^1_R t_L})}{2}(m^2_{t^1}+m_t^2-m_H^2)+2g_{Ht^1_R t_L}g_{Ht^1_L t_R}m_t m_{t^1}\right), \tag{66}$$

where

$$f(m_1, m_2, m_3) = \frac{1}{2m_1}\sqrt{m_1^4+m_2^4+m_3^4-2m_1^2m_2^2-2m_1^2m_3^2-2m_2^2m_3^2}. \tag{67}$$

We are taking the bottom mass to be negligible with respect to the other masses under consideration and we only consider $g_{W^+\bar{t}^1_L b_L}$ since $g_{W^+\bar{t}^1_R b_R} \ll g_{W^+\bar{t}^1_L b_L}$. For $m_{t^1} \gg m_t$, m_W, m_Z, m_H, it follows that $g_{Z\bar{t}^1_R t_R} \ll g_{Z\bar{t}^1_L t_L}$, $g_{H\bar{t}^1_L t_R} \ll g_{H\bar{t}^1_R t_L}$ and hence the expressions for the decay widths of t^1 reduce to

$$\Gamma_{Wt^1b} = \frac{g^2_{W^+\bar{t}^1_L b_L}}{32\pi}\frac{m^3_{t^1}}{m^2_W} \tag{68}$$

$$\Gamma_{Zt^1t} = \frac{g^2_{Z\bar{t}^1_L t_L}}{32\pi}\frac{m^3_{t^1}}{m^2_Z}f \tag{69}$$

$$\Gamma_{Ht^1t} = \frac{g^2_{Ht^1_R t_L}}{32\pi}m_{t^1}. \tag{70}$$

It is easy to see in this limiting case that the Goldstone equivalence theorem applies, by simply replacing in Eqs. (68)–(70) the analytical expressions for the couplings derived in Eqs. (60)–(62). One obtains a relation between the branching ratios of the decays of t^1 into W^+b, Zt, and Ht of approximately 2:1:1, implying that the main decay channel for t^1 will be through W^+b.

B. Numerical results

In Figs. 1 and 2, we have plotted the dependence of $g_{G^1\bar{t}t}$ and $g_{G^1\bar{t}^1t^1}$ on the bulk mass parameter c_1 which corresponds to the first multiplet. All the couplings were calculated in the linear regime for values of the parameter consistent with EWSB and EWPT. In Fig. 1 we notice that as c_1 goes to positive values, the left-handed and right-handed couplings of the top-quark approach each other and take values of the order of 2 times the strong gauge coupling. Moreover, we can see in Fig. 2 that, as c_1 becomes positive, $g_{G^1\bar{t}^1_R t^1_R}$ grows becoming similar in size to the approximately common value of the left- and right-handed $g_{G^1\bar{t}t}$. Furthermore, $g_{G^1\bar{t}^1_L t^1_L}$ remains approximately at a constant large value of about $2g_{G^1\bar{t}t}$ for positive c_1. In Fig. 3 we plot the behavior of the coupling $g_{Z\bar{t}^1t}$ as a function of m_{t^1}. As seen in this figure, the major contribution comes from the left-handed coupling to the fermions. Furthermore, we notice a dependence of $g_{Z\bar{t}^1_L t_L} \propto 1/m_{t^1}$, which can be understood by looking at Eq. (61) and taking into account that $m_{t^1} \propto \tilde{k}$. The $g_{W^+\bar{t}^1_L b_L}$ coupling shows a similar behavior.

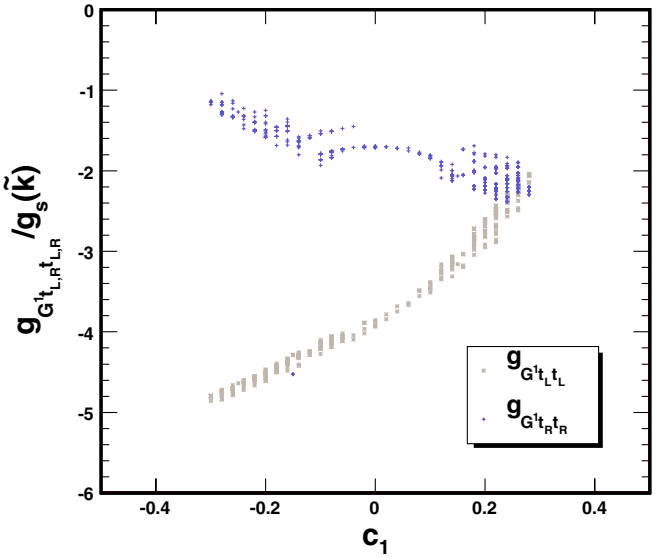

FIG. 1 (color online). $g_{G^1\bar{t}t}/g_s(\tilde{k})$ vs c_1. As c_1 grows, the coupling for both chiralities unifies.

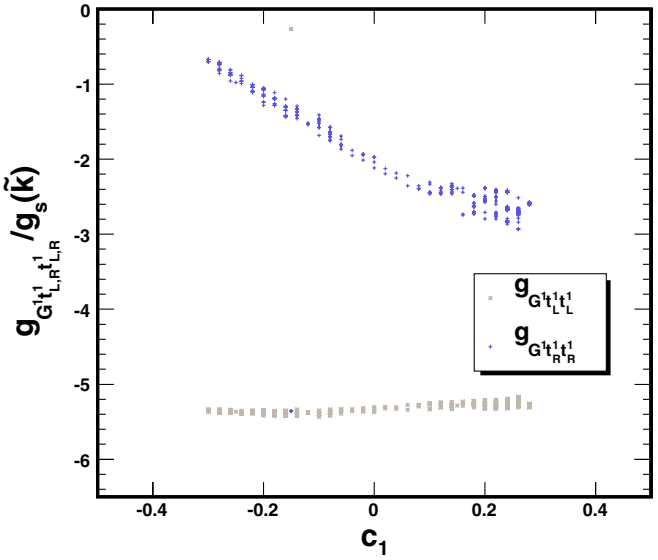

FIG. 2 (color online). $g_{G^1\bar{t}^1t^1}/g_s(\tilde{k})$ vs c_1. As c_1 grows, the left-handed coupling remains constant and the right-handed one grows.

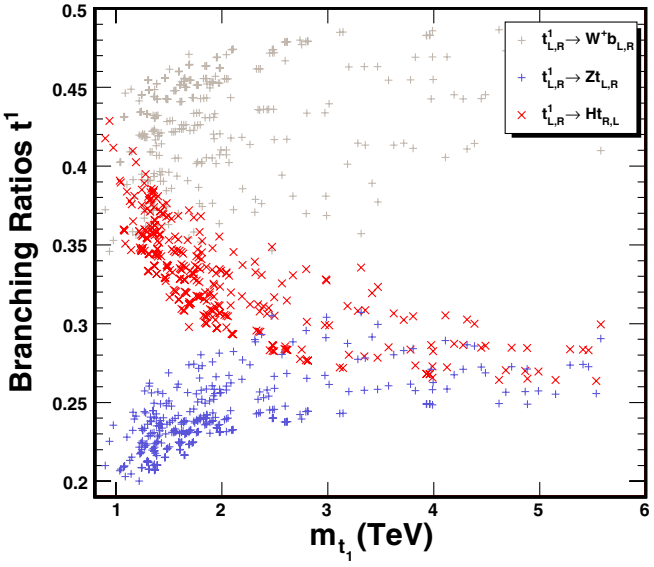

FIG. 4 (color online). Branching ratios for the decay of t^1 vs m_{t^1} (GeV). Notice that the 2:1:1 relations hold for large m_{t^1}

Apart from the couplings, as was previously discussed in Refs. [15,16,21], a very important property of this class of models is that the first excited state of the top quark is light enough as to enable the decay of G^1 into t^1 pairs. This property, together with the large coupling of G^1 to t^1's, implies a large branching ratio of the decay of G^1 into t^1 pairs. In Fig. 4 we show the branching ratio for the decay of t^1 into W^+b, Zt, and Ht. In this figure we can appreciate the appearance of the approximate 2:1:1 relation between the different branching ratios, consistent with the Goldstone equivalence theorem at large values for the masses of t^1. In Fig. 5 we observed, as predicted, the first

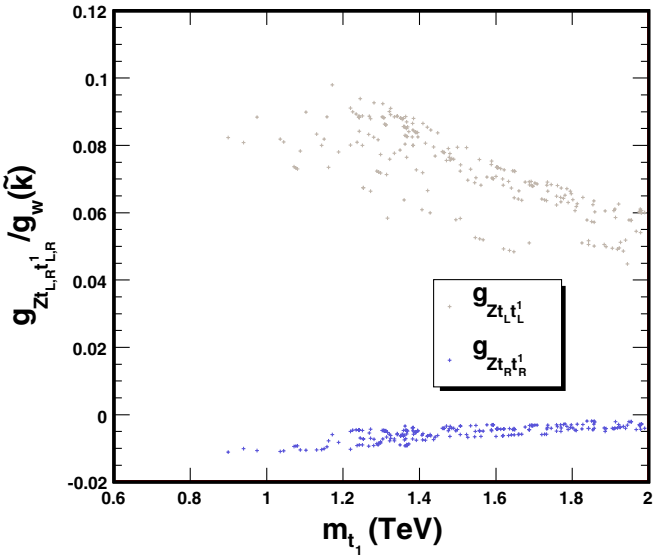

FIG. 3 (color online). $g_{Z\bar{t}^1t}/g_w(\tilde{k})$ vs m_{t^1} (TeV), where $g_w(\tilde{k}) = g_5/\sqrt{L}$. Notice the $1/m_{t^1}$ dependence of $g_{Z\bar{t}^1_Lt_L}$.

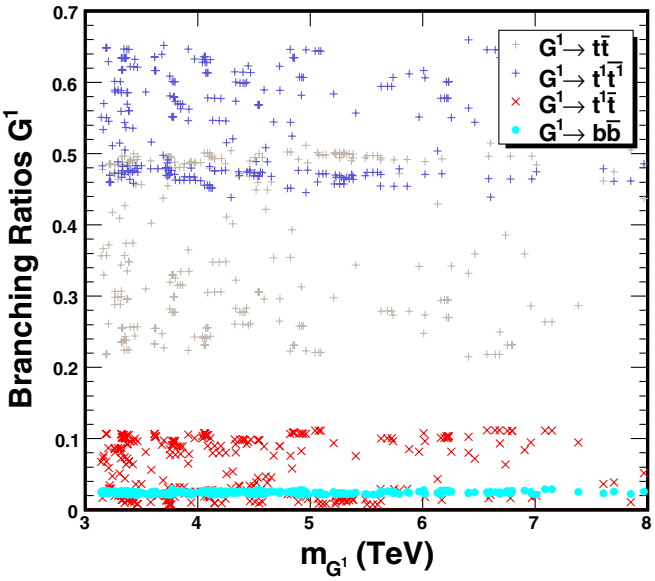

FIG. 5 (color online). Branching ratios for the decay of G^1 vs m_{G^1} (GeV). Notice that G^1 decays mostly to t^1 pairs.

KK excitation of the gluon decays mostly to t^1 pairs. The subsequent reduction of the branching ratio of the decay of G^1 into top-quark pairs, as well as large width effects, lead to important modifications of the collider phenomenology with respect to what has been studied in the literature [22–24], as we will discuss in detail in the next section.

VI. COLLIDER PHENOMENOLOGY

From the parameter space allowed in this kind of models, we see that the typical values for the masses of the first excited gauge bosons and third generation up-type fermion

Kaluza-Klein states are close to $2.5\tilde{k}$ and 0.8–$1.1\tilde{k}$, respectively. Values of $\tilde{k} \gtrsim 1.4$ TeV lead to consistency with precision electroweak observables and radiative electroweak symmetry breaking in the linear regime [15,16,21]. This leads to first excited KK gauge bosons with masses larger than about 3.5 TeV, whose wave functions are localized towards the IR brane. Since first and second generation fermions in these models are localized towards the UV brane, this implies a reduced coupling of these fermions to G^1, which turns out to be on the order of a fifth of the strong gauge coupling, rendering the search for these heavy G^1 states at the LHC challenging due to the relatively low production cross section.

Most of the previous studies of G^1 searches at the LHC have considered the case in which it predominantly decays into top-quark pairs [22–24]. As we stressed above, in the class of models analyzed in this article, which lead to consistency with precision electroweak data and electroweak symmetry breaking, the G^1 decays predominantly into t^1 pairs. Moreover, the total decay width of G^1 turns out to be in the range of 30% to 40% of the G^1 mass, which makes it a broad resonance leading to a harder analysis for the reconstruction of the G^1 mass. Therefore, in this work we shall analyze the search for the first excited fermion state of the top quark and concentrate on the relatively narrow t^1 mass reconstruction.

Searches for excited states of the top quark, decaying into third generation fermions and either Higgs or gauge bosons, have been the subject of intensive recent study in the literature. Assuming QCD production of these states, it has been shown that masses up to about 1 TeV may be tested at the LHC [27,28,30]. This range of masses, however, falls short of the necessary one to test the models under study, since the t^1-mass tends to be heavier than 1 TeV. In this work, we will make use of the increased production cross section of t^1 pairs induced by the presence of G^1's. As shown in [21], there is a strong correlation between the masses of the G^1 and the t^1 states, $m_{G^1} \approx (2.2$–$3)m_{t^1}$. For the G^1-masses allowed by precision measurements, $m_{G^1} \gtrsim 3$ TeV, the $m_{G^1} - m_{t^1}$ correlation leads to t^1 masses above 1 TeV. In Fig. 6, we show the different contributions to the t^1 pair production cross sections for a wide range of t^1 masses beyond those allowed in our model. We fix $m_{G^1} = 4$ TeV which corresponds in our framework to $m_{t^1} \sim 1.3$–1.8 TeV. It is precisely in this region of t^1 masses where the G^1 induced t^1 pair production cross section becomes larger than the QCD one. We notice in this figure that QCD production and G^1 induced production amplitudes interfere constructively. This can be understood, by noticing that, contrary to the QCD case, the coupling of the first excited KK gluon to t^1 pairs comes with an opposite sign to the coupling of G^1 to first and second generation quarks. In addition, most t^1 pairs are produced with an invariant mass smaller than m_{G^1}, leading to a constructive interference between both amplitudes due to the behavior of the gluon and G^1 propagators.

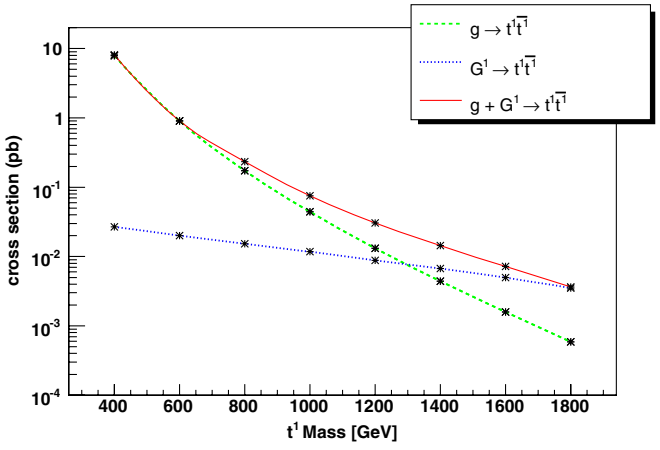

FIG. 6 (color online). Cross-section production at the LHC for $m_{G^1} = 4.0$ TeV with couplings $g_{G^1\bar{t}_L^1 t_L^1}/g_s(\tilde{k}) = -5.18$ and $g_{G^1\bar{t}_R^1 t_R^1}/g_s(\tilde{k}) = -2.77$.

With this in mind, we are going to show that it is possible to find a signal for t^1 with a mass up to about 1.5 TeV when we include the contribution to its production rate of the decay of a G^1 state with a mass of about 4 TeV in the high luminosity LHC era. We also consider a second point of 5D parameter space where the G^1-mass is of the order of 3.5 TeV and the t^1-mass is of order 1.25 TeV. We concentrate in a region of parameter space with $c_1 \geq 0$ where possible flavor changing operators are suppressed [25]. Moreover, as shown in Figs. 1 and 2, the suppressed couplings $g_{G^1\bar{t}_L t_L} \sim g_{G^1\bar{t}_R t_R}$ with respect to $g_{G^1\bar{t}_L^1 t_L^1}$ lead to a large branching ratio for t^1 production induced by G^1's. This can be appreciated in Fig. 5.

A. Signal and background simulation

We are interested in the study of a mostly $SU(2)_L$ singlet, vectorlike fermion state t^1, associated with the first KK resonance of charge $2/3$. This fermion state, due to gauge invariance, couples with regular SM QCD gluons with a strength given by the strong coupling and as stressed before, its signatures have been studied in detail in [27,28,30], showing a potential reach for these particles with a mass up to about $m_{t^1} \sim 1$ TeV.

As explained in the previous section, in the Gauge-Higgs unification models we are considering, the G^1 decays mostly to t^1's, and t^1 prefers to decay mainly in the W^+b channel. Thus, one of the best options to study this resonance is by means of the lepton + jets final state channel:

$$pp \to (g + G^1) \to t^1\bar{t}^1 \to W^+bW^-\bar{b} \to l^-\bar{\nu}b\bar{b}jj, \quad (l = e, \mu). \tag{71}$$

The jets include quarks of the first two families and the charge conjugated process is also considered. The irreducible backgrounds for this signal are coming from the SM by

means of $t\bar{t}$ production and W/Z + jets, and from the exotic $t\bar{t}$ production induced by G^1. As has been shown in [27,28], the W/Z + jets background can be reduced to negligible levels by requiring two b-tags and lepton + MET. In this work, we impose the above requirements and therefore concentrate on the analysis of the main background from $t\bar{t}$ production coming from both QCD and G^1.

We simulate the events for the background and signal at partonic level using the MADGRAPH-MADEVENT package v4.1.33 [34], which includes the HELAS [35] subroutine to compute the matrix elements. The renormalization scales for the QCD background are set at the top mass, and for the backgrounds $G^1 \to t\bar{t}$ and signal $G^1 \to t^1\bar{t}^1$ are set at the t^1-mass. Moreover, we choose the set CTEQ5l [36] for the structure functions. In order to reduce the amount of events that are produced in the background simulation due to the large QCD cross section, we put a mild cut at the generator level for the p_t of the lepton. This cut implies a weaker restriction in comparison to the cuts that we will implement in the analysis and therefore we do not introduce a bias over the background sample by implementing it at the generator level. For the signal, we put no cuts at the generator level and we produce almost 10 times more events than it is expected from the cross section. Therefore to obtain a realistic value in the counting of events, it is necessary to normalize to the correct value $\sigma\mathcal{L}$, where σ is the corresponding cross section and $\mathcal{L}$ is the LHC luminosity. This procedure allows us to obtain smooth profiles and simulate the results at higher luminosities.

The partonic level events produced by MADGRAPH are passed through the PYTHIA [37] and PGS 4 [38] packages included in MADGRAPH. The PYTHIA package performs the hadronization process and includes initial and final state radiation, where at this stage we use the default parameters that are included in PYTHIA. The PGS package performs a simulation of the LHC ATLAS detector based on a fit of the CDF data. We then modify the default parameters for the b-tag efficiencies in order to have a more realistic simulation for the high luminosity LHC era. To account for this, we replace the b-tag/mistag efficiencies with the set (1/2, 1/10, 1/30) for underlying b's, c's, and untagged jets (gluons and light quarks), respectively [28]. Furthermore, we set the jet cone reconstruction algorithm to $\Delta R = \sqrt{\Delta\eta^2 + \Delta\phi^2} = 0.6$ in order to optimize the reconstruction of the W mass from very collimated jets [28,30]. This choice of ΔR enhances the ratio of signal over background due to the kinematic differences between the W plus b jet system arising from these two processes. We will continue with the discussion of this subject in the analysis section, because it is found to be a key tool in the search for the t^1-resonance.

In Table I we specify the 5D parameters, associated couplings, and masses which we will use in the calculation of cross sections and t^1-mass reconstruction. We will denote the first set of parameters as point 1 and the second set as point 2. In Table II we show the values for the cross sections and number of events expected at the parton level for the different processes. One interesting aspect of this study as can be seen in Table II is the relatively large production cross section of top-quark pairs compared to t^1 pairs from G^1-induced production. That this occurs in spite of the fact that $\Gamma_{G^1tt} < \Gamma_{G^1t^1t^1}$ is a result of the relatively large width of the G^1 particle that leads to a strong departure from the narrow width approximation. Furthermore, enhancements of parton distribution functions at low x add to the width effects leading to a preference in the production of tops proceeding from G^1's at relatively low p_t. The invariant mass of most of the top-quark pairs produced from the G^1 decays is, therefore, much smaller than the G^1 mass. This can be seen clearly

TABLE I. Points of parameter space chosen for t^1 detection. All masses are given in GeV and the couplings are in units of $g_s(\tilde{k})$.

c_1	c_2	c_3	M_{B_1}	M_{B_2}	$h/(\sqrt{2}f_h)$	m_{G^1}	m_{t^1}	$g_{G^1\bar{t}t_R}$	$g_{G^1\bar{t}t_L}$	$g_{G^1\bar{t}^1t^1_R}$	$g_{G^1\bar{t}^1t^1_L}$
0.26	−0.41	−0.57	2.2	0.4	0.278	3915.8	1470.2	−2.09	−2.28	−2.73	−5.22
0.24	−0.41	−0.58	2.3	0.5	0.318	3439.6	1250.5	−2.12	−2.50	−2.67	−5.20

TABLE II. Value of the cross section at the parton level before cuts for final state $l^-\bar{\nu}b\bar{b}jj$ including the charge conjugated process, expected number of events, and number of events that pass the selection cuts in Eqs. (72) and (73), for point 1 at 300 fb^{-1} and point 2 at 100 fb^{-1}, respectively.

	Point 1			Point 2		
Process	σ [fb]	N^0 Events	N^0 after cuts	σ [fb]	N^0 Events	N^0 after cuts
$G^1 \to t\bar{t}$	4.12	1236	1	4.43	443	0
$g \to t^1\bar{t}^1$	0.23	70	5	0.687	69	5
$g + G^1 \to t\bar{t}$	3025	907 527	6	3085	308 509	6
$g + G^1 \to t^1\bar{t}^1$	0.88	266	21	2.015	201	13

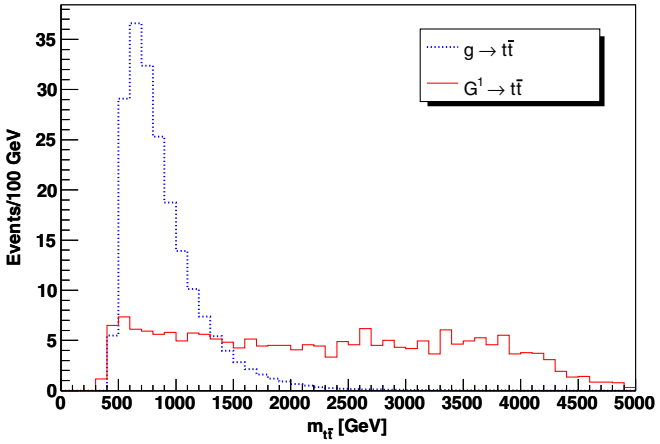

FIG. 7 (color online). $t\bar{t}$ invariant mass reconstruction from QCD and G^1 induced production for point 1. Distributions normalized to 200 events.

in Figs. 7 and 8, where both distributions have been normalized to a total of 200 events.

At this point we have not yet included the contribution of K-factors to the cross section. These K-factors take into account next to leading order (NLO) effects in the computation of the matrix elements, and their direct effect is to enhance the value of the cross section for all processes. In [28] it was shown that the signal to background ratio, for a heavy quark mass of ~600 GeV, computed with and without these K-factors is very similar. Moreover, in the computation of the K-factors obtained in Ref. [27], the enhancement of the NLO cross section with respect to the LO one increases with the mass of the heavy quark. It was obtained in Ref. [27] that $K(\bar{t}^1 t^1) \simeq 1.5$ and $K(\bar{t}t) \simeq 1.3$ for $m_{t^1} = 1$ TeV. Thus, we expect that the inclusion of these K-factors will enhance our amount of events and signal to background ratio. Even in the case in which the signal to background ratio remains approximately constant

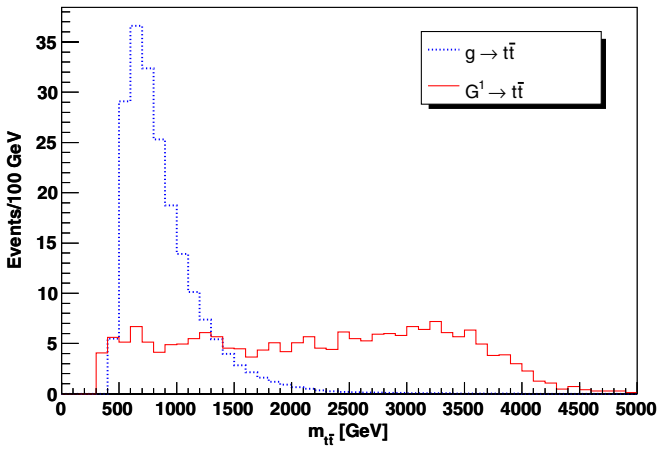

FIG. 8 (color online). $t\bar{t}$ invariant mass reconstruction from QCD and G^1 induced production for point 2. Distributions normalized to 200 events.

with the inclusion of K-factors, there is still an increase in the significance of about $\sqrt{K}$ that we will take into account at the end of our analysis.

B. Event selection

The first selection of the events is done at the level of hadronized particles. In order to study the properties of signal and background with sufficient statistics, we require that the hadronized events fulfill the following two criteria:

(i) Isolated lepton with $p_t > 20$ GeV and $|\eta| < 2.5$ plus missing energy with $p_t > 20$ GeV.

(ii) At least three jets with $p_t > 20$ GeV and $|\eta| < 2.5$, with exactly two bottom tags.

The lepton + MET requirements are useful to reduce the backgrounds from QCD jets, though we will put a stronger cut on the lepton p_t in the final analysis. The condition of exactly 2 b-tags is useful to reduce the backgrounds W/Z + jets although it leads to a strong reduction of the signal statistics.

From the numbers in Table II, it is clear that the cross section of the SM background is much bigger than the signal. Our approach to reduce backgrounds to manageable levels follows the one in [28]. We will put cuts over the p_t of the harder bottom and over H_t, the scalar sum of the p_t's. The distribution of these two variables for the background and signal are shown in Figs. 9–12. It is interesting to notice that the p_t distribution of t^1 without the presence of G^1 is similar to the same distribution including the G^1. From this behavior we conclude that, apart from the increase in the total production cross section, the analysis of the t^1 signal in this scenario would not differ significantly from the previous analysis in the search of heavy singlet quarks.

C. Analysis

To begin with, we would like to discuss the two different ways to reconstruct the W-mass from the hadronic jets

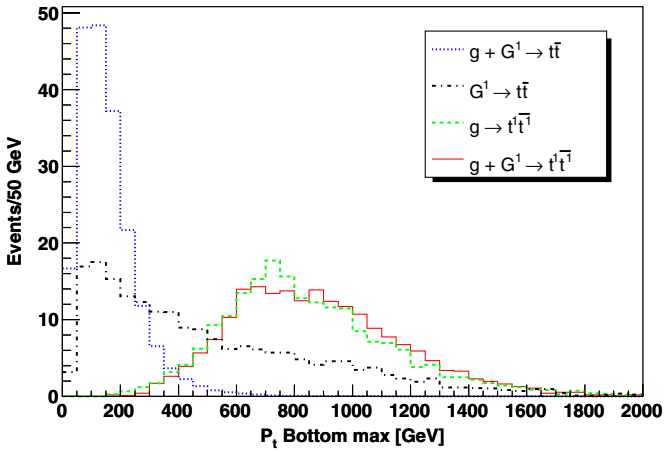

FIG. 9 (color online). p_t of the faster tagged bottom for point 1. Distribution normalized to 200 events.

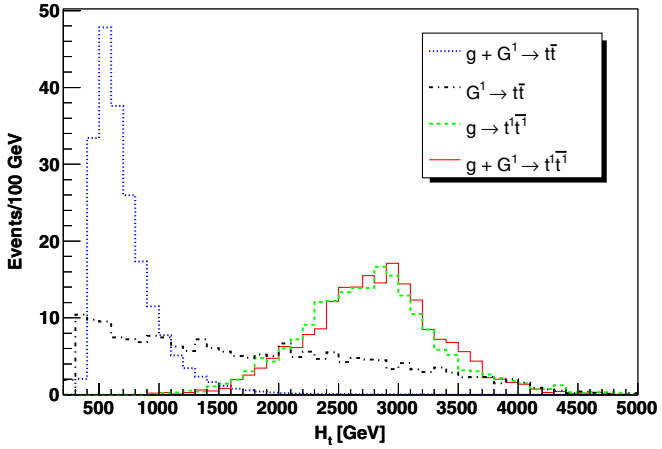

FIG. 10 (color online). Scalar sum of the all p_t for point 1. Distribution normalized to 200 events.

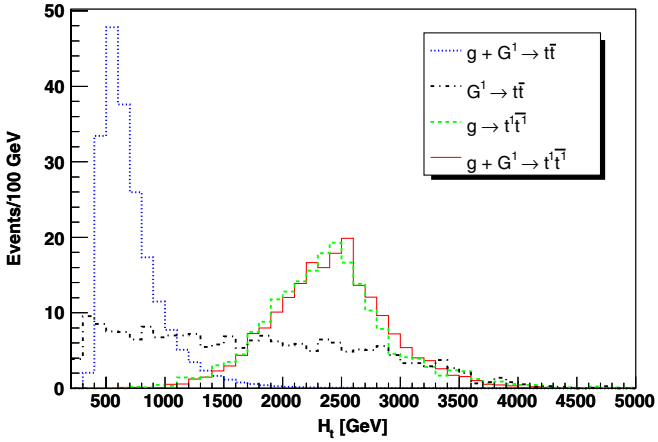

FIG. 12 (color online). Scalar sum of the all p_t for point 2. Distribution normalized to 200 events.

which are used in the literature to find this kind of resonances [27–29]. The first method is based in the direct search of the two jets coming from the W decay. The first jet is selected as the harder jet and the second one is the jet that forms an invariant mass with the first jet close to the W-mass. Thus, to optimize this procedure it is necessary to use a cone reconstruction algorithm with a $\Delta R \leq 0.4$ to avoid contamination from other jets. This method works very well when the events have W jets which are not too energetic, like in the $t\bar{t}$ background and in the signal when the t^1 masses are much smaller than 1 TeV [27]. The second method consists of reconstructing the W-mass using the harder jet information. This method is based on the kinematic behavior of the ultraenergetic jets coming from W's. These jets, coming from highly boosted W's, are so collimated that almost all of the W-jet energy is deposited in a cone of $\Delta R = 0.6$ around the E_t weighted barycenter [28]. In the scenario of heavy t^1's, like the ones present in our model, this method increases the signal and decreases the background. This is due to the fact that since the bottom produced from the SM energetic top quarks often contaminates the W-jets, then the reconstruction of the invariant W-mass is less efficient for the background and the opposite effect works for the signal, where the bottom and W-jet are not that much collimated because the heavy t^1 is produced almost at rest due to the broad G^1-width effect.

Figures 13–15 show the distribution of the reconstructed invariant W-mass using both methods; the plotted events are required to pass the first selection after PYTHIA-PGS level and $p_t^{j,\max} \geq 150$ GeV. To make the comparison more transparent, we use a cone algorithm with $\Delta R = 0.4$ for the first method and $\Delta R = 0.6$ for the second one. From these histograms it is clear that the more efficient method to reconstruct the invariant mass of the W coming from t^1 is the one that treats the W as a massive jet. Furthermore, we can use this behavior in the invariant mass of the faster jet to strongly reduce the background from $t\bar{t}$.

Using the information from the p_t and the invariant W-mass distribution for signal and background, we select

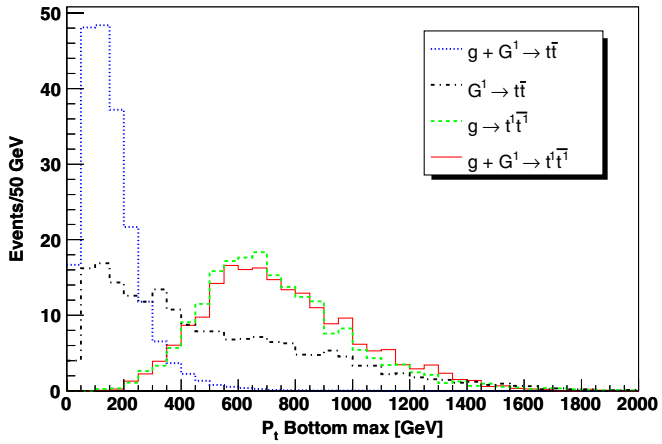

FIG. 11 (color online). p_t of the faster tagged bottom for point 2. Distribution normalized to 200 events.

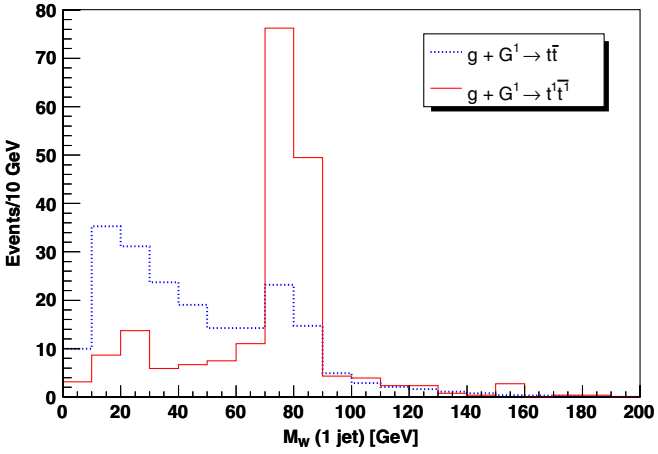

FIG. 13 (color online). Invariant reconstructed W mass using the method of only one jet for point 1. Distribution normalized to 200 events.

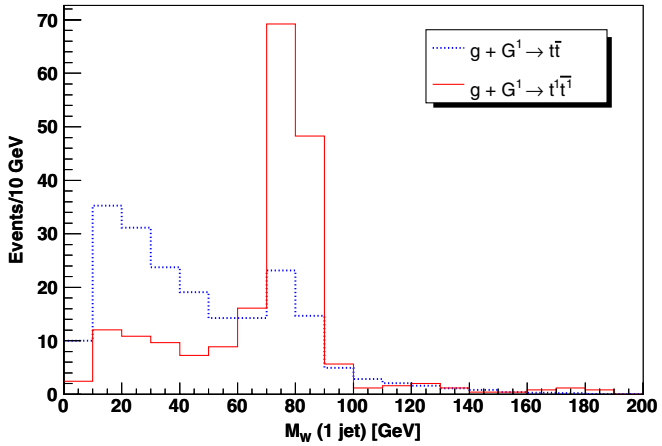

FIG. 14 (color online). Invariant reconstructed W mass using the method of only one jet for point 2. Distribution normalized to 200 events.

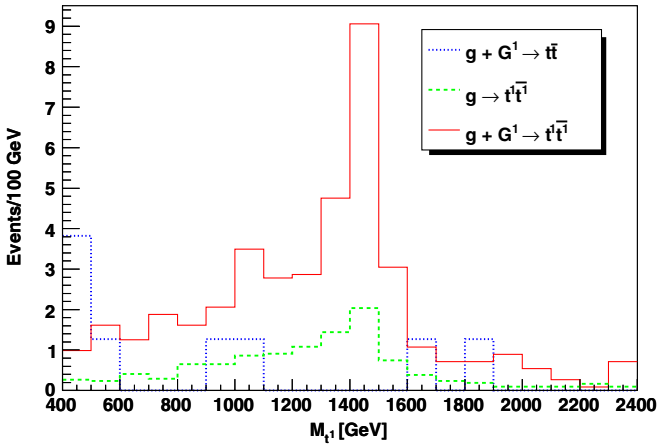

FIG. 16 (color online). Distribution of the t^1 mass reconstructed hadronically for point 1. The numbers of events represent the results after 300 fb^{-1} of LHC luminosity.

the next set of cuts to do the reconstruction of the t^1 mass distribution. In the case of $p_t^{b,\max}$ and H_t we use different cuts for point 1 (left column) and point 2 (right column), respectively,

$$\begin{aligned} p_t^{b,\max} &\geq 350 \text{ GeV}, & p_t^{b,\max} &\geq 300 \text{ GeV}, \\ H_t &\geq 1900 \text{ GeV}, & H_t &\geq 1800 \text{ GeV}, \\ p_t^{\text{lepton}} &\geq 200 \text{ GeV}, & p_t^{\text{lepton}} &\geq 150 \text{ GeV}. \end{aligned} \tag{72}$$

The remaining cuts are common to both points,

$$\begin{aligned} p_t^{j,\max} \geq 250 \text{ GeV}, \qquad |M_W - M_W^j| \leq 20 \text{ GeV}, \\ |m_{Wb_i} - m_t| \geq 50 \text{ GeV}, \end{aligned} \tag{73}$$

where m_{Wb_i} is the invariant mass of the Wb system and by b_i with $i = 1, 2$ we denote the two bottom quarks which come from the decay of either the t^1 or top pair system. As was mentioned before, the cut in the lepton p_t is imposed in order to reduce the $\bar{t}t$ background, but leads to a strong reduction of the signal. The cut in $p_t^{j,\max}$ strongly reduces the background while leaving the signal after the first cut almost intact. The last cut strongly reduces the background as well. This can be understood since in the $t - \bar{t}$ background case, at least one of the bottoms tends to reconstruct the top-quark mass with the W gauge boson; something that does not happen with the signal. The relevance of the other cuts has been discussed above.

We present in Figs. 16 and 17 the reconstructed invariant mass m_{t^1} vs the number of reconstructed t^1's per 100 GeV for both signal and background at 300 fb^{-1} of LHC luminosity for point 1 and at 100 fb^{-1} for point 2. In both cases we notice an accumulation of events with an invariant mass close to the physical mass of the t^1 particles, leading to the first hint of a heavy quark with a relevant branching ratio decay in the W^+b channel. It is apparent from both figures

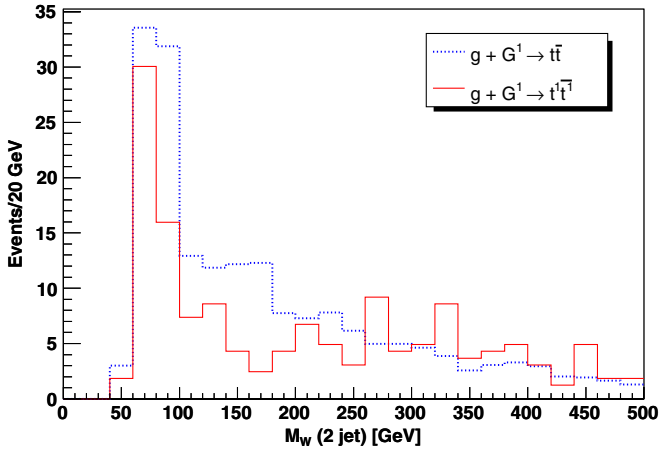

FIG. 15 (color online). Invariant reconstructed W mass using the method of two jets, for point 1 (similar results for point 2). Distribution normalized to 200 events.

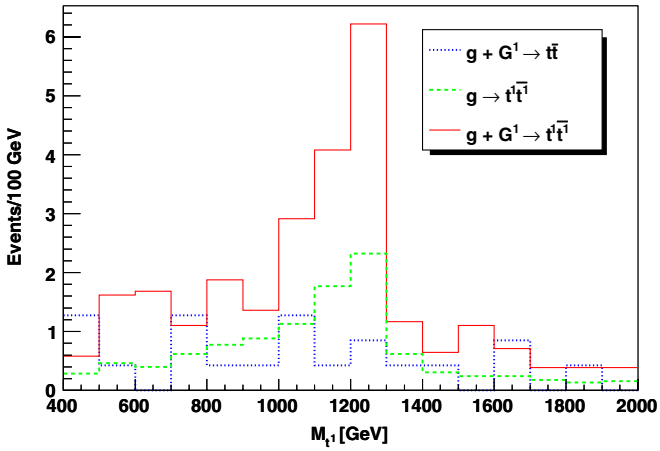

FIG. 17 (color online). Distribution of the t^1 mass reconstructed hadronically for point 2. The numbers of events represent the results after 100 fb^{-1} of LHC luminosity.

that the background has a much flatter distribution in the same mass range after cuts. Following Ref. [28], we have considered all W b pairs in each event. This leads to an increase in statistics by doubling the number of points per event and furthermore a broadening of the reconstructed mass distribution.

In order to distinguish among the bottom quarks which we use to reconstruct the t^1 resonance, we can impose a further requirement. We will choose the bottom which has the biggest ΔR with respect to the W gauge boson. This requirement is imposed because the bottom quark and the W's coming from t^1 decays usually have a large angular separation since t^1's are produced mostly at low p_t. This will lead to a preference of real reconstructed t^1's compared to fake ones in the signal events. We plot in Figs. 18 and 19 the reconstructed invariant mass m_{t^1} vs the number of reconstructed t^1's per 100 GeV for both signal and background at 300 fb^{-1} of LHC luminosity for point 1 and at 100 fb^{-1} for point 2, with this new requirement.

In order to estimate the statistical significance of the excess of signal over background for points 1 and 2 at the respective luminosities, we take into account the total number of events of signal (S) and background (B) obtained after cuts. Assuming a Poisson distribution of signal and background events, the statistical significance would be given by $S/\sqrt{S+B}$. Using the numbers in Table II for points 1 and 2, we estimate a statistical significance $S/\sqrt{S+B} \sim 4.04\sigma$ at a luminosity of 300 fb^{-1} and $S/\sqrt{S+B} \sim 2.98\sigma$ at a luminosity of 100 fb^{-1}, respectively. As mentioned before, the inclusion of K-factors will tend to increase the total significance of the signal. Taking values of the K-factors of roughly 1.5 for both signal and background, we obtain a 5σ significance for point 1 at 300 fb^{-1}. For point 2, instead, t^1-discovery cannot be achieved even after the inclusion of K-factors at a luminosity of 100 fb^{-1}. However, an increase in luminosity up

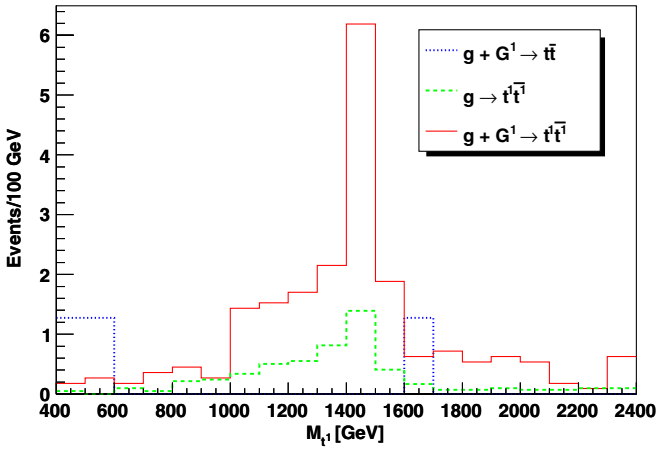

FIG. 18 (color online). Distribution of the t^1 mass reconstructed hadronically for point 1. The numbers of events represent the results after 300 fb^{-1} of LHC luminosity, with the additional requirement of ΔR in the Wb system.

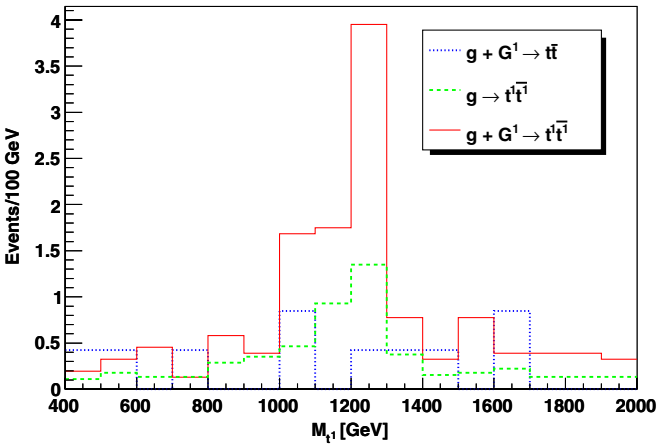

FIG. 19 (color online). Distribution of the t^1 mass reconstructed hadronically for point 2. The numbers of events represent the results after 100 fb^{-1} of LHC luminosity, with the additional requirement of ΔR in the Wb system.

to about 200 fb^{-1} will be sufficient to discover t^1 at 5σ significance.

An improved analysis based on an exhaustive treatment of physics and nonphysics backgrounds, with further optimization of the cuts, inclusion of NLO QCD corrections, and a more realistic detector simulation should be done to confirm these results. Keeping this in mind, our preliminary results indicate that, after including K-factors, 3σ evidence for the presence of these particles may be found already at 100 fb^{-1} (60 fb^{-1}) and that 5σ discovery can be achieved with about 300 fb^{-1} (200 fb^{-1}) for points 1 and 2, respectively. Figures 18 and 19 clearly show the importance of the contribution of G^1's in t^1 production (and detection), by comparing the number of events produced by the process $g + G^1 \rightarrow \bar{t}^1 t^1$ with the ones produced by the process $g \rightarrow \bar{t}^1 t^1$. If we only had direct QCD production the signal would be overwhelmed by the background.

In order to explore the last point further, we have done a simulation considering only QCD production of t^1 pairs at the LHC with a luminosity of 300 fb^{-1}. Assuming the biggest branching ratio into the $W^+ b$ channel for a given t^1-mass as seen in Fig. 4 ($BR_{W^+ b} \approx 0.45$), using the massive jet technique and similar cuts and efficiencies as was done in the previous simulations, we found that the maximum t^1-mass which can be reconstructed leading to a 5σ discovery at the LHC is $m_{t^1} \approx 1.1$ TeV. This corresponds to a t^1 production cross section of about 30 fb. Similarly, for point 1 we have shown that by considering G^1-induced production of t^1 in addition to QCD production at a luminosity of 300 fb^{-1}, the LHC will be sensitive to t^1 masses up to about 1.5 TeV. This corresponds to a t^1 production cross section of about 15 fb as presented in Fig. 6. Though the cross section for point 1 is half the value of the pure QCD cross section necessary to discover a 1.1 TeV t^1, the difference can be understood by the increase in the efficiency of the cuts at high mass.

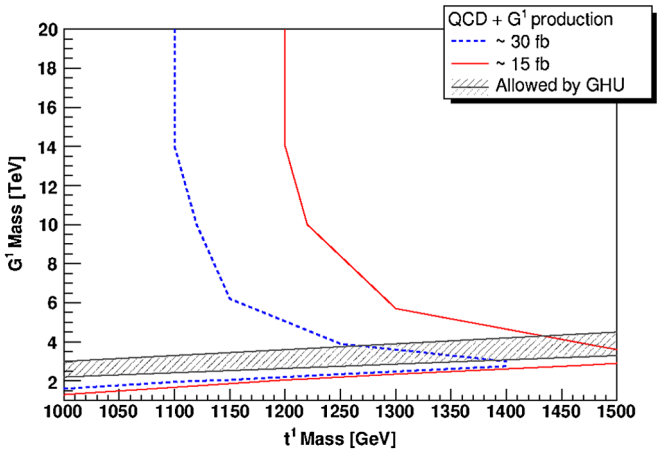

FIG. 20 (color online). Curves of constant cross section for QCD in addition of G^1 decay, in the (m_{G^1}, m_{t^1}) plane.

We can use the above information to obtain an estimate of the reach of the LHC at 300 fb^{-1} for arbitrary m_{t^1} and m_{G^1} masses. In Fig. 20 we show the curves representing the points in the (m_{G^1}, m_{t^1}) plane with constant cross section of either 30 fb (blue dotted line) or 15 fb (red solid line). The lower bounds in the figure correspond to phase suppression due to the impossibility of producing t^1's from G^1-decays. For masses $m_{G^1} \to +\infty$, the blue curve approaches the maximum value for t^1-masses that can be tested by QCD production alone. All points between the upper and lower blue and red lines have a cross section larger than 30 fb and 15 fb, respectively. Since the efficiency of the cuts tends to increase with large t^1-masses, one expects that the LHC will be able to explore the whole region bounded by the lower and upper blue curves with $m_{t^1} \geq 1.1$ TeV. This, however, underestimates the full reach of the LHC since it does not take into account the increase in cut efficiency at large t^1 masses. The real sensitivity curve for the case of G^1-induced production in addition to QCD production, will lie in between the upper red and blue curves, interpolating the points $(+\infty, 1.1$ TeV) and (4 TeV, 1.5 TeV) in (m_{G^1}, m_{t^1}) space. The shaded area in Fig. 20 represents the region of allowed G^1 and t^1 masses in the Gauge-Higgs unification models considered in the previous sections. We can see from the figure that the LHC at 300 fb^{-1} will be able to probe a large region of parameter space for these type of models which are consistent with electroweak symmetry breaking and electroweak precision tests.

D. Discussion and outlook

Let us close this section by discussing some important points related to the search for the t^1 resonance. In the analysis above, we have considered a flat 0.5 b-tagging efficiency, independent of the p_t of the tagged jet. This may be an optimistic assumption, particularly at the early stages of the LHC. The search for the heavy t^1's analyzed in this work, however, will require high LHC luminosity. If the LHC b-tagging efficiency at high p_t for 2 b-tagged jets proves to be lower than the one assumed in this work, it may be helpful to perform the search without b-tagging requirements. This will increase both signal and background, particularly the W plus jets background. The cut on the p_t of the harder jet and the massive W-jet, and the requirement of a high-p_t lepton and large missing energy may be sufficient to reduce the background to manageable levels. The results of Ref. [29] seem promising in this direction.

In this work, we have only analyzed the search for the t^1-quark in its W plus b decay mode. However, as discussed above, t^1 decays about half of the time into a top quark and either a Higgs or a Z-gauge boson. For the large t^1 masses we considered in this work, the decay products will be highly boosted and therefore the reconstruction of these particles will be most efficient by using the technique of massive jets. It would be useful to analyze the LHC reach in the search for t^1's including these alternative decay modes.

Single t^1 production is a complimentary production channel to the one discussed in this work and has been analyzed in the context of the little Higgs model [39,40]. Similar to the $\bar{t}^1 t^1$ production induced by G^1, the single t^1 production cross section also becomes larger than the QCD t^1 pair production cross section for sufficiently large values of the t^1 masses. The study of Ref. shows that the t^1 single production extends the sensitivity to t^1 masses at the LHC well above those reachable via the QCD process. It would be interesting to analyze single t^1 production in detail in our specific model. In addition to likely extending the reach for the t^1 mass, this could also provide information about the Wt^1b coupling.

One important property of the Gauge-Higgs unification model analyzed in this article is the suppression of the Higgs production cross section in both the W-fusion and gluon fusion modes [16,18,21,41–43]. The reduction of the Higgs boson coupling to gluons could imply the presence of extra scalar states that mix with the Higgs and/or of extra colored states. In the class of Gauge-Higgs unification models under analysis, the t^1 will provide the dominant contribution to the gluon fusion amplitude in addition to the top quark. In this sense, the discovery of the heavy t^1 mode, and the study of its properties, may be essential in order to understand Higgs boson production at the LHC.

VII. CONCLUSIONS

We have analyzed the possible detection at the LHC of excited states of the top quark in Gauge-Higgs unification models in warped extra dimensions that are consistent with radiative electroweak symmetry breaking and precision electroweak measurements. In these models, the t^1 tends to be strongly coupled to the first gluon excitation G^1 and sufficiently light, so that it can be produced from decays of G^1. This reduces the branching ratio of the decay of G^1 into

top quarks and enhances the width of G^1, making its reconstruction from top decays difficult. On the other hand, consistency with precision measurements may only be obtained for masses of t^1 larger than about 1 TeV.

After presenting a consistent functional method for the computation of the couplings of the fermion modes to the gauge modes, we computed the relevant decay widths necessary for the collider phenomenology analysis. An immediate consequence of the heaviness of the t^1 is that its decay branching ratios into W^+b, tZ, and tH states are in an approximate 2:1:1 relation which becomes a better approximation with increasing t^1-mass. On the other hand, for the large t^1 masses we considered, $m_{t^1} > 1$ TeV, the SM decay products tend to be boosted, making the reconstruction of the weak gauge bosons from its decay into quarks very difficult. Instead, as recently emphasized in the literature, it is convenient to apply the technique of massive jets, that becomes essential for an efficient reconstruction of the t^1 states in our case.

Our analysis shows that the increase in the production cross section of t^1 pairs, induced by the presence of G^1's in the class of models under analysis, extends the reach of the t^1 searches to masses not accessible via direct QCD production. There is a strong correlation between the G^1 and t^1 masses, and we obtain that for a value of m_{G^1} of about 4 TeV and with a high LHC luminosity of about 300 fb^{-1}, the first KK excitation of the top quark with a mass of 1.5 TeV may be detected. The discovery of a t^1 in this mass range, possible due to an increase in its production cross section, may point towards the presence of a heavy gauge boson resonance contributing to the t^1 production rate. It may be possible to obtain information about the G^1 resonance from the analysis of t^1 production. Moreover, while t^1 induces a suppression of the Higgs production via gluon fusion, the study of the additional decay channel of t^1 into Higgs and a top quark may lead to novel Higgs production signatures at the LHC. In summary, the search of a singlet vectorlike heavy quark pair produced at the LHC opens the possibility to explore the parameter space of Gauge-Higgs unification models consistent with precision electroweak measurements and electroweak symmetry breaking.

ACKNOWLEDGMENTS

We would like to thank Adam Falkowski, Ayres Freitas, Jay Hubisz, Tom LeCompte, Ben Lillie, Ian Low, Eduardo Ponton, Jose Santiago, Jing Shu, and Tim Tait for useful discussions and comments. Work at ANL is supported in part by the U.S. DOE, Division of HEP, Contract No. DE-AC02-06CH11357. This work was also supported in part by the U.S. Department of Energy through Grant No. DE-FG02-90ER40560. B. P. work was supported in part by CONICYT, Chile.

APPENDIX A: $SO(5)$ GENERATORS

The generators of the fundamental representation of $SO(5)$, with $\mathrm{Tr}[\mathrm{T}^\alpha \cdot \mathrm{T}^\beta] = \mathrm{C}(5)\delta^{\alpha\beta}$, are given by

$$T^{a_{\mathrm{L,R}}}_{i,j} = -\frac{i\sqrt{C(5)}}{2}\left[\frac{1}{2}\epsilon^{abc}(\delta^b_i\delta^c_j - \delta^b_j\delta^c_i) \pm (\delta^a_i\delta^4_j - \delta^a_j\delta^4_i)\right],$$

$$T^{\hat{a}}_{i,j} = -i\sqrt{\frac{C(5)}{2}}(\delta^{\hat{a}}_i\delta^5_j - \delta^{\hat{a}}_j\delta^5_i), \tag{A1}$$

where $T^{\hat{a}}$ ($\hat{a} = 1, 2, 3, 4$) and $T^{a_{\mathrm{L,R}}}$ ($a_{\mathrm{L,R}} = 1,2, 3$) are the generators of $SO(5)/SO(4)$ and $SO(4)$, respectively.

Define the matrices A and B as follows, which gives us the generators in the basis that T^{3_L} and T^{3_R} are diagonal:

$$A = \frac{1}{\sqrt{2}}\begin{pmatrix} -i & -1 & 0 & 0 & 0 \\ 0 & 0 & -i & 1 & 0 \\ 0 & 0 & i & 1 & 0 \\ -i & 1 & 0 & 0 & 0 \\ 0 & 0 & 0 & 0 & \sqrt{2} \end{pmatrix} \tag{A2}$$

$$B = \frac{1}{\sqrt{2}}\begin{pmatrix} i & 1 & 0 & 0 & 0 & 0 & 0 & 0 & 0 & 0 \\ 0 & 0 & -i & 1 & 0 & 0 & 0 & 0 & 0 & 0 \\ 0 & 0 & -i & -1 & 0 & 0 & 0 & 0 & 0 & 0 \\ -i & 1 & 0 & 0 & 0 & 0 & 0 & 0 & 0 & 0 \\ 0 & 0 & 0 & 0 & -1 & i & 0 & 0 & 0 & 0 \\ 0 & 0 & 0 & 0 & 0 & 0 & \sqrt{2} & 0 & 0 & 0 \\ 0 & 0 & 0 & 0 & 1 & i & 0 & 0 & 0 & 0 \\ 0 & 0 & 0 & 0 & 0 & 0 & 0 & -1 & i & 0 \\ 0 & 0 & 0 & 0 & 0 & 0 & 0 & 0 & 0 & \sqrt{2} \\ 0 & 0 & 0 & 0 & 0 & 0 & 0 & 1 & i & 0 \end{pmatrix}. \tag{A3}$$

The generators used in the text should always be understood to be related to the ones defined above as $A \cdot T^\alpha \cdot A^\dagger$ for the fundamental representation and $B \cdot T^\alpha \cdot B^\dagger$ for the adjoint representation.

APPENDIX B: GAUGE AND FERMION WAVE FUNCTIONS WITH $h \neq 0$

It should be understood in the following that all the previously defined functions, $S_{\pm M_i}$, $\dot{S}_{\pm M_i}$, S, and C are functions of x_5 and z, where $z = m_n$ and m_n is taken to be the mass of the particle of interest. The functions θ_{Gx} and θ_{Fx} are defined as

$$\theta_{Gx} = \frac{\lambda_G h f_h}{f_{hx}^2}, \tag{B1}$$

$$\theta_{Fx} = \frac{\lambda_F h f_h}{f_{hx}^2}, \tag{B2}$$

where

$$f_{hx}^2 = \frac{1}{g_5^2 \int_0^{x_5} dy a^{-2}(y)}. \tag{B3}$$

The gauge boson wave functions in the presence of the Higgs vev are as follows:

$$f_{G,\hat{a}}(x_5, h) = \begin{bmatrix} (\cos\theta_{G_x} C_{G,\hat{1}} + \frac{1}{\sqrt{2}} \sin\theta_{G_x} C_{G,1_R}) S[x] - \frac{1}{\sqrt{2}} \sin\theta_{G_x} C_{G,1_L} C[x] \\ (\cos\theta_{G_x} C_{G,\hat{2}} + \frac{1}{\sqrt{2}} \sin\theta_{G_x} C_{G,2_R}) S[x] - \frac{1}{\sqrt{2}} \sin\theta_{G_x} C_{G,2_L} C[x] \\ \cos\theta_{G_x} C_{G,\hat{3}} S[x] + \frac{1}{\sqrt{2}} \sin\theta_{G_x} (c_\phi C_{G,3_R} S[x] + (s_\phi C_{G,Y} - C_{G,3_L}) C[x]) \\ S[x] C_{G,\hat{4}} \end{bmatrix} \tag{B4}$$

$$f_{G,a_L}(x_5, h) = \begin{bmatrix} \frac{1}{2}((1 + \cos\theta_{G_x}) C_{G,1_L} C[x] + (\sqrt{2} \sin\theta_{G_x} C_{G,\hat{1}} + (1 - \cos\theta_{G_x}) C_{G,1_R}) S[x]) \\ \frac{1}{2}((1 + \cos\theta_{G_x}) C_{G,2_L} C[x] + (\sqrt{2} \sin\theta_{G_x} C_{G,\hat{2}} + (1 - \cos\theta_{G_x}) C_{G,2_R}) S[x]) \\ \frac{1}{2}(((1 - \cos\theta_{G_x}) c_\phi C_{G,3_R} + \sqrt{2} \sin\theta_{G_x} C_{G,\hat{3}}) S[x] + ((1 + \cos\theta_{G_x}) C_{G,3_L} + (1 - \cos\theta_{G_x}) s_\phi C_{G,Y}) C[x]) \end{bmatrix} \tag{B5}$$

$$f_{G,a_R}(x_5, h) = \begin{bmatrix} \frac{1}{2}((1 - \cos\theta_{G_x}) C_{G,1_L} C[x] - (\sqrt{2} \sin\theta_{G_x} C_{G,\hat{1}} - (1 + \cos\theta_{G_x}) C_{G,1_R}) S[x]) \\ \frac{1}{2}((1 - \cos\theta_{G_x}) C_{G,2_L} C[x] - (\sqrt{2} \sin\theta_{G_x} C_{G,\hat{2}} - (1 + \cos\theta_{G_x}) C_{G,2_R}) S[x]) \\ \frac{1}{2}(((1 + \cos\theta_{G_x}) c_\phi C_{G,3_R} - \sqrt{2} \sin\theta_{G_x} C_{G,\hat{3}}) S[x] + ((1 - \cos\theta_{G_x}) C_{G,3_L} + (1 + \cos\theta_{G_x}) s_\phi C_{G,Y}) C[x]) \end{bmatrix} \tag{B6}$$

$$f_{G,X}(x_5, h) = [\, c_\phi C_{G,Y} C[x] - s_\phi C_{G,3_R} S[x] \,]. \tag{B7}$$

The fermion wave functions in the presence of the Higgs vev are given by the following:

$$f_{F,1,L}(x_5, h) = \begin{bmatrix} C_{F,1} S_{M_1} \\ \frac{1}{2}((1 + \cos\theta_{F_x}) C_{F,2} S_{M_1} - (1 - \cos\theta_{F_x}) C_{F,3} \dot{S}_{-M_1} - \sqrt{2} \sin\theta_{F_x} C_{F,5} S_{M_1}) \\ \frac{1}{2}((1 + \cos\theta_{F_x}) C_{F,3} \dot{S}_{-M_1} - (1 - \cos\theta_{F_x}) C_{F,2} S_{M_1} - \sqrt{2} \sin\theta_{F_x} C_{F,5} S_{M_1}) \\ C_{F,4} \dot{S}_{-M_1} \\ \frac{1}{\sqrt{2}} \sin\theta_{F_x} (C_{F,2} S_{M_1} + C_{F,3} \dot{S}_{-M_1}) + \cos\theta_{F_x} C_{F,5} S_{M_1} \end{bmatrix} \tag{B8}$$

$$f_{F,2,R}(x_5, h) = \begin{bmatrix} C_{F,6} S_{-M_2} \\ \frac{1}{2}((1 + \cos\theta_{F_x}) C_{F,7} S_{-M_2} - (1 - \cos\theta_{F_x}) C_{F,8} S_{-M_2} - \sqrt{2} \sin\theta_{F_x} C_{F,10} \dot{S}_{M_2}) \\ \frac{1}{2}((1 + \cos\theta_{F_x}) C_{F,8} S_{-M_2} - (1 - \cos\theta_{F_x}) C_{F,7} S_{-M_2} - \sqrt{2} \sin\theta_{F_x} C_{F,10} \dot{S}_{M_2}) \\ C_{F,9} S_{-M_2} \\ \frac{1}{\sqrt{2}} \sin\theta_{F_x} (C_{F,7} + C_{F,8}) S_{-M_2} + \cos\theta_{F_x} C_{F,10} \dot{S}_{M_2} \end{bmatrix} \tag{B9}$$

$$f_{F,3,R}(x_5,h)=\begin{bmatrix}\cos\theta_{F_x}C_{F,11}S_{-M_3}-\frac{i}{\sqrt{2}}\sin\theta_{F_x}(C_{F,15}-C_{F,18})S_{-M_3}\\ \frac{1}{2}((1+\cos\theta_{F_x})C_{F,12}-(1-\cos\theta_{F_x})C_{F,13}-i\sin\theta_{F_x}(C_{F,16}-C_{F,19}))S_{-M_3}\\ \frac{1}{2}((1+\cos\theta_{F_x})C_{F,13}-(1-\cos\theta_{F_x})C_{F,12}-i\sin\theta_{F_x}(C_{F,16}-C_{F,19}))S_{-M_3}\\ \cos\theta_{F_x}C_{F,14}S_{-M_3}-\frac{i}{\sqrt{2}}\sin\theta_{F_x}(C_{F,17}S_{-M_3}-C_{F,20}\dot{S}_{M_3})\\ \frac{1}{2}((1+\cos\theta_{F_x})C_{F,15}+(1-\cos\theta_{F_x})C_{F,18}-i\sqrt{2}\sin\theta_{F_x}C_{F,11})S_{-M_3}\\ \frac{1}{2}((1+\cos\theta_{F_x})C_{F,16}+(1-\cos\theta_{F_x})C_{F,19}-i\sin\theta_{F_x}(C_{F,12}+C_{F,13}))S_{-M_3}\\ \frac{1}{2}((1+\cos\theta_{F_x})C_{F,17}S_{-M_3}+(1-\cos\theta_{F_x})C_{F,20}\dot{S}_{M_3}-i\sqrt{2}\sin\theta_{F_x}C_{F,14}S_{-M_3})\\ \frac{1}{2}(i\sqrt{2}\sin\theta_{F_x}C_{F,11}+(1-\cos\theta_{F_x})C_{F,15}+(1+\cos\theta_{F_x})C_{F,18})S_{-M_3}\\ \frac{1}{2}(i\sin\theta_{F_x}(C_{F,12}+C_{F,13})+(1-\cos\theta_{F_x})C_{F,16}+(1+\cos\theta_{F_x})C_{F,19})S_{-M_3}\\ \frac{1}{2}(i\sqrt{2}\sin\theta_{F_x}C_{F,14}S_{-M_3}+(1-\cos\theta_{F_x})C_{F,17}S_{-M_3}+(1+\cos\theta_{F_x})C_{F,20}\dot{S}_{M_3})\end{bmatrix}. \tag{B10}$$

The boundary equations separate by charge as said previously. For the $5/3$ charge $C_{F,1}$, $C_{F,11}$, $C_{F,15}$, and $C_{F,18}$ is one coupled sets given by

$$2C_{F,1}\dot{S}_{M_1}[L]+M_{B_2}\left(2\cos\left[\frac{\lambda_F h}{f_h}\right]C_{F,11}+i\sqrt{2}\sin\left[\frac{\lambda_F h}{f_h}\right](C_{F,15}-C_{F,18})\right)S_{-M_3}[L]=0, \tag{B11}$$

$$2M_{B_2}C_{F,1}S_{M_1}[L]-\left(2\cos\left[\frac{\lambda_F h}{f_h}\right]C_{F,11}+i\sqrt{2}\sin\left[\frac{\lambda_F h}{f_h}\right](C_{F,15}-C_{F,18})\right)\dot{S}_{-M_3}[L]=0, \tag{B12}$$

$$\left(i\sqrt{2}\sin\left[\frac{\lambda_F h}{f_h}\right]C_{F,11}+\left(1+\cos\left[\frac{\lambda_F h}{f_h}\right]\right)C_{F,15}+\left(1-\cos\left[\frac{\lambda_F h}{f_h}\right]\right)C_{F,18}\right)\dot{S}_{-M_3}[L]=0, \tag{B13}$$

$$\left(-i\sqrt{2}\sin\left[\frac{\lambda_F h}{f_h}\right]C_{F,11}+\left(1-\cos\left[\frac{\lambda_F h}{f_h}\right]\right)C_{F,15}+\left(1+\cos\left[\frac{\lambda_F h}{f_h}\right]\right)C_{F,18}\right)\dot{S}_{-M_3}[L]=0, \tag{B14}$$

the equation involving $C_{F,6}$ is independent. The $-1/3$ charged fermions are also given by two sets: $C_{F,4}$, $C_{F,14}$, $C_{F,17}$, $C_{F,2}$ which includes the bottom,

$$2C_{F,4}S_{-M_1}[L]+M_{B_2}\left(2\cos\left[\frac{\lambda_F h}{f_h}\right]C_{F,14}S_{-M_3}[L]+i\sqrt{2}\sin\left[\frac{\lambda_F h}{f_h}\right](C_{F,17}S_{-M_3}[L]-C_{F,20}\dot{S}_{M_3}[L])\right)=0, \tag{B15}$$

$$2\left(\cos\left[\frac{\lambda_F h}{f_h}\right]C_{F,14}\dot{S}_{-M_3}[L]-M_{B_2}C_{F,4}\dot{S}_{-M_1}[L]\right)-i\sqrt{2}\sin\left[\frac{\lambda_F h}{f_h}\right](C_{F,20}S_{M_3}[L]-C_{F,17}\dot{S}_{-M_3}[L])=0, \tag{B16}$$

$$\left(1-\cos\left[\frac{\lambda_F h}{f_h}\right]\right)C_{F,20}S_{M_3}[L]+\left(i\sqrt{2}\sin\left[\frac{\lambda_F h}{f_h}\right]C_{F,14}+\left(1+\cos\left[\frac{\lambda_F h}{f_h}\right]\right)C_{F,17}\right)\dot{S}_{-M_3}[L]=0, \tag{B17}$$

$$\left(1+\cos\left[\frac{\lambda_F h}{f_h}\right]\right)C_{F,20}S_{M_3}[L]+\left(-i\sqrt{2}\sin\left[\frac{\lambda_F h}{f_h}\right]C_{F,14}+\left(1-\cos\left[\frac{\lambda_F h}{f_h}\right]\right)C_{F,17}\right)\dot{S}_{-M_3}[L]=0, \tag{B18}$$

and one independently $C_{F,9}$.

The set for the charge $2/3$ fermion involves $C_{F,2}$, $C_{F,3}$, $C_{F,5}$, $C_{F,7}$, $C_{F,8}$, $C_{F,10}$, $C_{F,12}$, $C_{F,13}$, $C_{F,16}$, $C_{F,19}$, which includes the top and is given by

$$\begin{aligned}M_{B_2}\Bigg(\left(1+\cos\left[\frac{\lambda_F h}{f_h}\right]\right)C_{F,12}-\left(1-\cos\left[\frac{\lambda_F h}{f_h}\right]\right)C_{F,13}+i\sin\left[\frac{\lambda_F h}{f_h}\right](C_{F,16}-C_{F,19})\Bigg)S_{-M_3}[L]\\ -\left(1-\cos\left[\frac{\lambda_F h}{f_h}\right]\right)C_{F,3}S_{-M_1}[L]+\left(\left(1+\cos\left[\frac{\lambda_F h}{f_h}\right]\right)C_{F,2}-\sqrt{2}\sin\left[\frac{\lambda_F h}{f_h}\right]C_{F,5}\right)\dot{S}_{M_1}[L]=0,\end{aligned} \tag{B19}$$

$$M_{B_2}\left(\left(1-\cos\left[\frac{\lambda_F h}{f_h}\right]\right)C_{F,12}-\left(1+\cos\left[\frac{\lambda_F h}{f_h}\right]\right)C_{F,13}-i\sin\left[\frac{\lambda_F h}{f_h}\right](C_{F,16}-C_{F,19})\right)S_{-M_3}[L]$$
$$-\left(1+\cos\left[\frac{\lambda_F h}{f_h}\right]\right)C_{F,3}S_{-M_1}[L]+\left(\left(1-\cos\left[\frac{\lambda_F h}{f_h}\right]\right)C_{F,2}+\sqrt{2}\sin\left[\frac{\lambda_F h}{f_h}\right]C_{F,5}\right)\dot{S}_{M_1}[L]=0, \quad \text{(B20)}$$

$$\sin\left[\frac{\lambda_F h}{f_h}\right](C_{F,3}S_{-M_1}[L]+M_{B_1}(C_{F,7}+C_{F,8})S_{-M_2}[L]+C_{F,2}\dot{S}_{M_1}[L])+\sqrt{2}\cos\left[\frac{\lambda_F h}{f_h}\right](C_{F,5}\dot{S}_{M_1}[L]+M_{B_1}C_{F,10}\dot{S}_{M_2}[L])=0, \quad \text{(B21)}$$

$$\sin\left[\frac{\lambda_F h}{f_h}\right](-M_{B_1}(C_{F,2}S_{M_1}[L]+C_{F,3}\dot{S}_{-M_1}[L])+(C_{F,7}+C_{F,8})\dot{S}_{-M_2}[L])$$
$$-\sqrt{2}\cos\left[\frac{\lambda_F h}{f_h}\right](M_{B_1}C_{F,5}S_{M_1}[L]-C_{F,10}S_{M_2}[L])=0, \quad \text{(B22)}$$

$$\sqrt{2}\sin\left[\frac{\lambda_F h}{f_h}\right]C_{F,10}S_{M_2}[L]-\left(\left(1+\cos\left[\frac{\lambda_F h}{f_h}\right]\right)C_{F,7}-\left(1-\cos\left[\frac{\lambda_F h}{f_h}\right]\right)C_{F,8}\right)\dot{S}_{-M_2}[L]=0, \quad \text{(B23)}$$

$$\sqrt{2}\sin\left[\frac{\lambda_F h}{f_h}\right]C_{F,10}S_{M_2}[L]+\left(\left(1-\cos\left[\frac{\lambda_F h}{f_h}\right]\right)C_{F,7}-\left(1+\cos\left[\frac{\lambda_F h}{f_h}\right]\right)C_{F,8}\right)\dot{S}_{-M_2}[L]=0, \quad \text{(B24)}$$

$$M_{B_2}\left(\left(\left(1+\cos\left[\frac{\lambda_F h}{f_h}\right]\right)C_{F,2}-\sqrt{2}\sin\left[\frac{\lambda_F h}{f_h}\right]C_{F,5}\right)S_{M_1}[L]-\left(1-\cos\left[\frac{\lambda_F h}{f_h}\right]\right)C_{F,3}\dot{S}_{-M_1}[L]\right)$$
$$-\left(\left(1+\cos\left[\frac{\lambda_F h}{f_h}\right]\right)C_{F,12}-\left(1-\cos\left[\frac{\lambda_F h}{f_h}\right]\right)C_{F,13}+i\sin\left[\frac{\lambda_F h}{f_h}\right](C_{F,16}-C_{F,19})\right)\dot{S}_{-M_3}[L]=0, \quad \text{(B25)}$$

$$M_{B_2}\left(\left(\left(1-\cos\left[\frac{\lambda_F h}{f_h}\right]\right)C_{F,2}+\sqrt{2}\sin\left[\frac{\lambda_F h}{f_h}\right]C_{F,5}\right)S_{M_1}[L]-\left(1+\cos\left[\frac{\lambda_F h}{f_h}\right]\right)C_{F,3}\dot{S}_{-M_1}[L]\right)$$
$$-\left(\left(1-\cos\left[\frac{\lambda_F h}{f_h}\right]\right)C_{F,12}-\left(1+\cos\left[\frac{\lambda_F h}{f_h}\right]\right)C_{F,13}-i\sin\left[\frac{\lambda_F h}{f_h}\right](C_{F,16}-C_{F,19})\right)\dot{S}_{-M_3}[L]=0, \quad \text{(B26)}$$

$$\left(i\sin\left[\frac{\lambda_F h}{f_h}\right](C_{F,12}+C_{F,13})+\left(1+\cos\left[\frac{\lambda_F h}{f_h}\right]\right)C_{F,16}+\left(1-\cos\left[\frac{\lambda_F h}{f_h}\right]\right)C_{F,19}\right)\dot{S}_{-M_3}[L]=0, \quad \text{(B27)}$$

$$\left(i\sin\left[\frac{\lambda_F h}{f_h}\right](C_{F,12}+C_{F,13})-\left(1-\cos\left[\frac{\lambda_F h}{f_h}\right]\right)C_{F,16}-\left(1+\cos\left[\frac{\lambda_F h}{f_h}\right]\right)C_{F,19}\right)\dot{S}_{-M_3}[L]=0. \quad \text{(B28)}$$

[1] L. Randall and R. Sundrum, Phys. Rev. Lett. **83**, 3370 (1999).
[2] N. Arkani-Hamed and M. Schmaltz, Phys. Rev. D **61**, 033005 (2000).
[3] T. Gherghetta and A. Pomarol, Nucl. Phys. **B586**, 141 (2000);
[4] S. J. Huber and Q. Shafi, Phys. Lett. B **498**, 256 (2001).
[5] H. Davoudiasl, J. L. Hewett, and T. G. Rizzo, Phys. Lett. B **473**, 43 (2000).
[6] S. Chang, J. Hisano, H. Nakano, N. Okada, and M. Yamaguchi, Phys. Rev. D **62**, 084025 (2000).
[7] K. Agashe and R. Contino, Nucl. Phys. **B742**, 59 (2006).
[8] C. Csaki, J. Erlich, and J. Terning, Phys. Rev. D **66**, 064021 (2002).
[9] J. L. Hewett, F. J. Petriello, and T. G. Rizzo, J. High Energy Phys. 09 (2002) 030.
[10] G. Burdman and Y. Nomura, Nucl. Phys. **B656**, 3 (2003).
[11] H. Davoudiasl, J. L. Hewett, and T. G. Rizzo, Phys. Rev. D **68**, 045002 (2003).
[12] M. S. Carena, A. Delgado, E. Ponton, T. M. P. Tait, and C. E. M. Wagner, Phys. Rev. D **71**, 015010 (2005).
[13] K. Agashe, A. Delgado, M. J. May, and R. Sundrum, J. High Energy Phys. 08 (2003) 050.

[14] K. Agashe, R. Contino, L. Da Rold, and A. Pomarol, Phys. Lett. B **641**, 62 (2006).
[15] M. Carena, E. Ponton, J. Santiago, and C. E. M. Wagner, Nucl. Phys. **B759**, 202 (2006).
[16] M. S. Carena, E. Ponton, J. Santiago, and C. E. M. Wagner, Phys. Rev. D **76**, 035006 (2007).
[17] K. Agashe, R. Contino, and A. Pomarol, Nucl. Phys. **B719**, 165 (2005).
[18] Y. Sakamura and Y. Hosotani, Phys. Lett. B **645**, 442 (2007).
[19] N. S. Manton, Nucl. Phys. **B158**, 141 (1979); Y. Hosotani, Phys. Lett. **126B**, 309 (1983); H. Hatanaka, T. Inami, and C. S. Lim, Mod. Phys. Lett. A **13**, 2601 (1998); I. Antoniadis, K. Benakli, and M. Quiros, New J. Phys. **3**, 20 (2001); M. Kubo, C. S. Lim, and H. Yamashita, Mod. Phys. Lett. A **17**, 2249 (2002); C. Csaki, C. Grojean, and H. Murayama, Phys. Rev. D **67**, 085012 (2003); N. Haba, M. Harada, Y. Hosotani, and Y. Kawamura, Nucl. Phys. **B657**, 169 (2003); **B669**, 381(E) (2003); C. A. Scrucca, M. Serone, and L. Silvestrini, Nucl. Phys. **B669**, 128 (2003); R. Contino, Y. Nomura, and A. Pomarol, Nucl. Phys. **B671**, 148 (2003).
[20] R. Contino, L. Da Rold, and A. Pomarol, Phys. Rev. D **75**, 055014 (2007).
[21] A. D. Medina, N. R. Shah, and C. E. M. Wagner, Phys. Rev. D **76**, 095010 (2007).
[22] K. Agashe, A. Belyaev, T. Krupovnickas, G. Perez, and J. Virzi, Phys. Rev. D **77**, 015003 (2008).
[23] B. Lillie, L. Randall, and L. T. Wang, J. High Energy Phys. 09 (2007) 074.
[24] B. Lillie, J. Shu, and T. M. P. Tait, Phys. Rev. D **76**, 115016 (2007).
[25] K. Agashe, G. Perez, and A. Soni, Phys. Rev. D **75**, 015002 (2007).
[26] A. Djouadi, G. Moreau, and R. K. Singh, arXiv:0706.4191.
[27] J. A. Aguilar-Saavedra, Phys. Lett. B **625**, 234 (2005); **633**, 792 (2006).
[28] B. Holdom, J. High Energy Phys. 03 (2007) 063.
[29] B. Holdom, J. High Energy Phys. 08 (2007) 069.
[30] W. Skiba and D. Tucker-Smith, Phys. Rev. D **75**, 115010 (2007).
[31] Y. Hosotani and M. Mabe, Phys. Lett. B **615**, 257 (2005).
[32] A. Falkowski, Phys. Rev. D **75**, 025017 (2007).
[33] A. Pomarol, Phys. Lett. B **486**, 153 (2000).
[34] F. Maltoni and T. Stelzer, J. High Energy Phys. 02 (2003) 027.
[35] E. Murayama, I. Watanabe, and K. Hagiwara, KEK Report No 91-11, 1992.
[36] H. L. Lai *et al.* (CTEQ Collaboration), Eur. Phys. J. C **12**, 375 (2000).
[37] T. Sjostrand, S. Mrenna, and P. Skands, J. High Energy Phys. 05 (2006) 026.
[38] J. Conway *et al.*, http://www.physics.ucdavis.edu/conway/research/software/pgs/pgs4-general.htm.
[39] G. Azuelos *et al.*, Eur. Phys. J. C **39S2**, 13 (2005).
[40] T. Han, H. E. Logan, and L. T. Wang, J. High Energy Phys. 01 (2006) 099.
[41] A. Falkowski, arXiv:0711.0828 [Phys. Rev. D (to be published)].
[42] A. Djouadi and G. Moreau, Phys. Lett. B **660**, 67 (2008).
[43] N. Maru and N. Okada, Phys. Rev. D **77**, 055010 (2008).